THESIS FOR THE DEGREE OF DOCTOR OF PHILOSOPHY

Effect of metal and cubic carbide additions on interface chemistry, phase composition and grain growth in WC-Co based cemented carbides

JONATHAN WEIDOW

Department of Applied Physics

CHALMERS UNIVERSITY OF TECHNOLOGY

Göteborg, Sweden 2010

Effect of metal and cubic carbide additions on interface chemistry, phase composition and grain growth in WC-Co based cemented carbides
JONATHAN WEIDOW
ISBN 978-91-7385-394-1

Doktorsavhandlingar vid Chalmers tekniska högskola
Ny serie nr 3075
ISSN 0346-718X

Department of Applied Physics
Chalmers University of Technology
SE-412 96 Göteborg
Sweden
Email: jonathan.weidow@chalmers.se

Cover: Left image shows a TEM micrograph of an APT specimen of a WC-TaC-Co cemented carbide. Right image shows an APT reconstruction of the same specimen. Green dots = W atoms, red = C, blue = Co, pink = Ta.

Printed by:
Chalmers Reproservice
Göteborg, Sweden 2010

Effect of metal and cubic carbide additions on interface chemistry, phase composition and grain growth in WC-Co based cemented carbides

JONATHAN WEIDOW

Department of Applied Physics
Chalmers University of Technology

ABSTRACT

A cemented carbide is a composite material used in metal cutting operations. A hardness providing WC-based skeleton is embedded in a toughness providing binder, mainly consisting of Co. The material is produced by powder metallurgical methods. Additions to the powder mixture are often made of grain growth inhibitors such as V or Cr, in order to retain a fine grained WC, and cubic carbides such as TiC, ZrC, NbC or TaC, in order to increase the material wear resistance.

Two series of materials were produced. In the first series, small amounts of V, Cr or Mn were added, and in the second series, larger amounts of TiC, ZrC, NbC or TaC were added. The microstructure of the two series was investigated with scanning electron microscopy, transmission electron microscopy and atom probe tomography. In this study, the effects the additions have on interface chemistry, phase composition and grain growth are systematically investigated.

Segregation corresponding to between one half and one monolayer of close packed Co was observed to WC/WC grain boundaries as well as to WC/(M,W)C phase boundaries. For the grain boundaries, some of the Co atoms were replaced of Ti, V, Cr, Mn, Fe, Zr, or Nb but not Ni or Ta. Segregation corresponding to approximately one monolayer of close packed VC was observed to WC/binder phase boundaries. Segregation of Ti, V, Cr, Mn, Zr, Nb and Ta to the WC/binder phases corresponding to less than one monolayer close packed MC was also observed.

Of the investigated additions, Ta had the highest solubility in WC, followed by Nb, Cr and V, all with atom fraction solubilities in the 10^{-3}-range. Mn and Ti showed lower, yet detectable, solubilities in the 10^{-6} or 10^{-5}-range. The solubilities of Co and Zr were too low to be measured.

All additions inhibited WC grain growth. For the first series of materials, V was the most efficient grain growth inhibitor with a mean WC grain size that was 38 % smaller than for a corresponding reference material. For the second series of materials, Ti was most efficient with a mean WC grain size that was 40 % smaller than for a corresponding reference material.

Keywords: SEM, TEM, EBSD, EDX, APT

Preface

The work presented in this thesis was mainly carried out at the Division of Microscopy and Microanalysis, Department of Applied Physics, Chalmers University of Technology, during the period 2005-2010 under the supervision of Prof. Hans-Olof Andrén.

The following six papers are included in the thesis:

I. Effect of V, Cr and Mn additions on the microstructure of WC-Co
J. Weidow, S. Norgren, H.-O. Andrén
International Journal of Refractory Metals & Hard Materials, 2009, 27, 817-822

II. Grain and phase boundary segregation in WC-Co with small V, Cr or Mn additions
J. Weidow, H.-O. Andrén
Acta Materialia, in press

III. Characterisation of WC-Co with cubic carbide additions
J. Weidow, J. Zackrisson, B. Jansson, H.-O. Andrén
International Journal of Refractory Metals & Hard Materials, 2009, 27, 244-248

IV. Grain and phase boundary segregation in WC-Co with TiC, ZrC, NbC or TaC additions
J. Weidow, H.-O. Andrén
Submitted to International Journal of Refractory Metals & Hard Materials

V. Transition metal solubilities in WC in cemented carbide materials
J. Weidow, S. Johansson, H.-O. Andrén, G. Wahnström
Submitted to Journal of the American Ceramic Society

VI. Binder phase grain size and binder grain boundary segregation in WC-Co based cemented carbides
J. Weidow, H.-O. Andrén
In manuscript

The materials analysed in my papers were manufactured by Sandvik Tooling AB and Seco Tools AB. All production control measurements were performed at the companies and I participated in some of these. Apart from this, my contribution to the papers is as follows:

I. I made all the experimental work and wrote the paper.

II. I made all the experimental work and wrote the paper.

III. I made all the experimental work and wrote the paper.

IV. I made all the experimental work and wrote the paper.

V. I made all the experimental work and wrote the paper with Sven Johansson, who made the modelling work.

VI. I made all the experimental work and wrote the paper.

I have also been co-author of four papers that either overlap the work in the included papers or deal with the details of TEM specimen preparation. They are therefore not included:

Effect of manganese on the microstructure of cemented carbides

J. Weidow, S. Norgren, M. Elfwing, H.-O. Andrén
Extended abstracts of 2006 Powder Metallurgy World Congress, Seoul, South Korea, 2006, Part 1, 348-349

3DAP analysis of interfaces in WC-Co systems

J. Weidow, H.-O. Andrén
Proceedings of Microscopy Society of Southern Africa, Ondestepoort, South Africa, 2006, 36, 23

Analysis of interfaces in WC-Co with cubic carbide additions

J. Weidow, H.-O. Andrén, B. Jansson, J. Zackrisson, S. Norgren
Proceedings of the 17th Plansee Seminar, Volders, Austria, 2009, Part 2, HM3

Nanometer scale site-specific *in situ* lift-out procedure

H. Pettersson, S. Mousavi Nik, J. Weidow, E. Olsson
To be submitted to Ultramicroscopy

Contents

1 Introduction

In the manufacturing industry, there is a need for fast and reliable metal cutting operations such as turning (Fig. 1), drilling and milling. An increase in the productivity of these operations can have dramatic positive economic effect, especially if the alternative is to hire more staff or increase the number of machines in the production. For this reason, it is of big importance to get deeper knowledge of the materials being used as cutting tools and learn how to improve them.

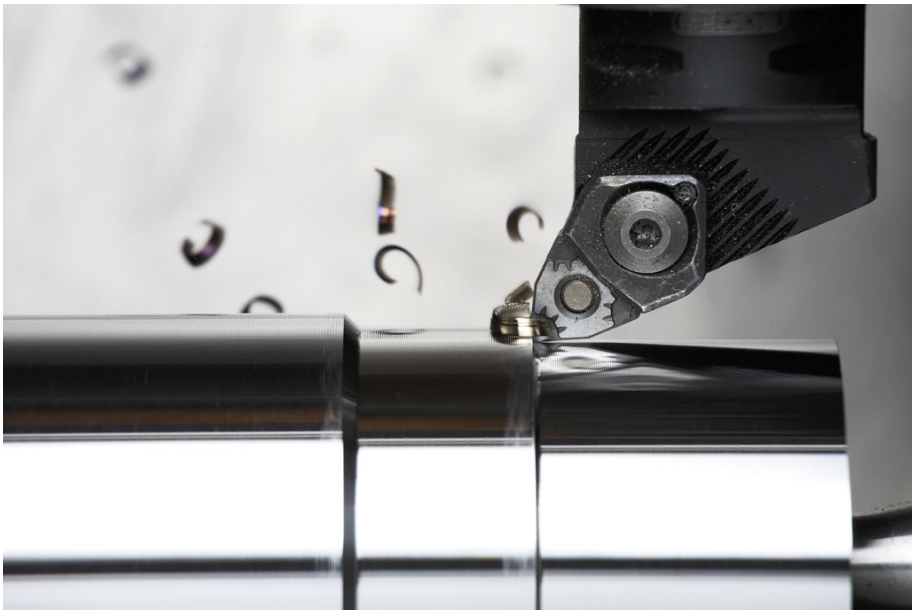

Figure 1: Insert made of cemented carbide in a turning operation. Courtesy Seco Tools AB.

Cemented carbide is a suitable type of tool material for metal cutting operations due to its high hot hardness, relatively high toughness and good wear resistance. The material consists of a hardness providing WC-based skeleton embedded in a toughness providing binder, most often mainly consisting of Co. The material is produced by powder metallurgical methods. During sintering, powders from the different constituents are bound to each other and the material is densified. During sintering WC grain growth is also taking place, thus changing the material properties. In order to decrease the grain growth, various grain growth inhibitors are added to the powder mixture. Addition of one or more cubic carbides, MC, to the powder mixture increases the wear resistance of the material.

1.1 Aim

The underlying reason for grain growth inhibition is not completely known. As a grain will grow against, and on the expense on, another grain or against the binder phase, it is of great interest to analyse the microstructure of WC/WC grain boundaries as well as WC/binder phase boundaries in cemented carbides. This could help us to better understand the grain growth inhibiting process. Since the hard phase skeleton is held together at the WC/WC grain boundaries, and at WC/MC interfaces if a MC phase exist in the material, it is also of great interest to investigate the microstructure of these interfaces to understand the strength of the skeleton.

With this work, it is the aim to systematically examine the impact different additions have on the microstructure of WC-Co based cemented carbides. This includes an investigation of the chemistry of different interfaces, an analysis of the phase compositions and a quantitatative analysis of grain growth in the material systems. The hope is to better understand the grain growth inhibiting mechanism as well as the strength of the material when used in cutting operations.

2 Cemented carbides

2.1 History

During the First World War, the Allied had a blockade against German import. Among the products that thereby were difficult to get were diamond needed for drawing dies for the production of tungsten filaments in the electrical industry [1]. The problem was solved by K. Schröter and F. Skaupy from Osram Studiengesellschaft in the early 1920s with the first patent from 1923 [2]-[3]. WC and Co powder were mixed, compacted and heated above the melting point of Co [3]. The first commercial product name for cemented carbides came from Fried Krupp in Germany and was Widia (like diamond) [2]. Metal cutting operations that earlier took 26 minutes with high speed steel tools now only took 6 minutes with the first cemented carbide tools [4]. In the beginning of the cemented carbide history, there were problems with wear at cutting operations of steel caused by carbon diffusion [4]. This problem was solved within a couple of years by the addition of TiC, NbC or TaC powder to the powder mixture [2]-[4]. It was also discovered that the addition of more than one carbide to the material had beneficial effects [2]. In the 1930s and 1940s, cemented carbides with smaller WC grain size, some with Cr_3C_2 powder added to the powder mixture, were developed [2]. The introduction of coatings in the early 1960s dramatically increased the tool life time as a result of decrease of wear [1]-[2][4].

Today, cemented carbides are challenged by materials such as polycrystalline diamond, cubic boron nitride, ceramics and high speed steel when it comes to choosing a material for metal cutting operations. Some of these material are harder than cemented carbides and some are tougher. However, the combination of high hot hardness, high toughness and good wear resistance makes cemented carbides the first hand choice in many occasions.

2.2 Manufacturing

Producing cemented carbides is everything but easy. WC dissociates at 2800 °C [3] and therefore, powder metallurgy is mainly used (Fig. 2). The sintering process also gives other advantages such as a possibility to, at least to some extent, control the grain size of the material.

Powder production

The required amounts of the different powder constituents are weighed and put in a mill. In addition, a pressing aid, such as paraffin wax or polyethylene glycol (PEG), as well as a milling aid that will minimize temperature rise and prevent oxidation, such as acetone or ethanol, are added to the mixture [2]. The purpose of the milling is to mix the different

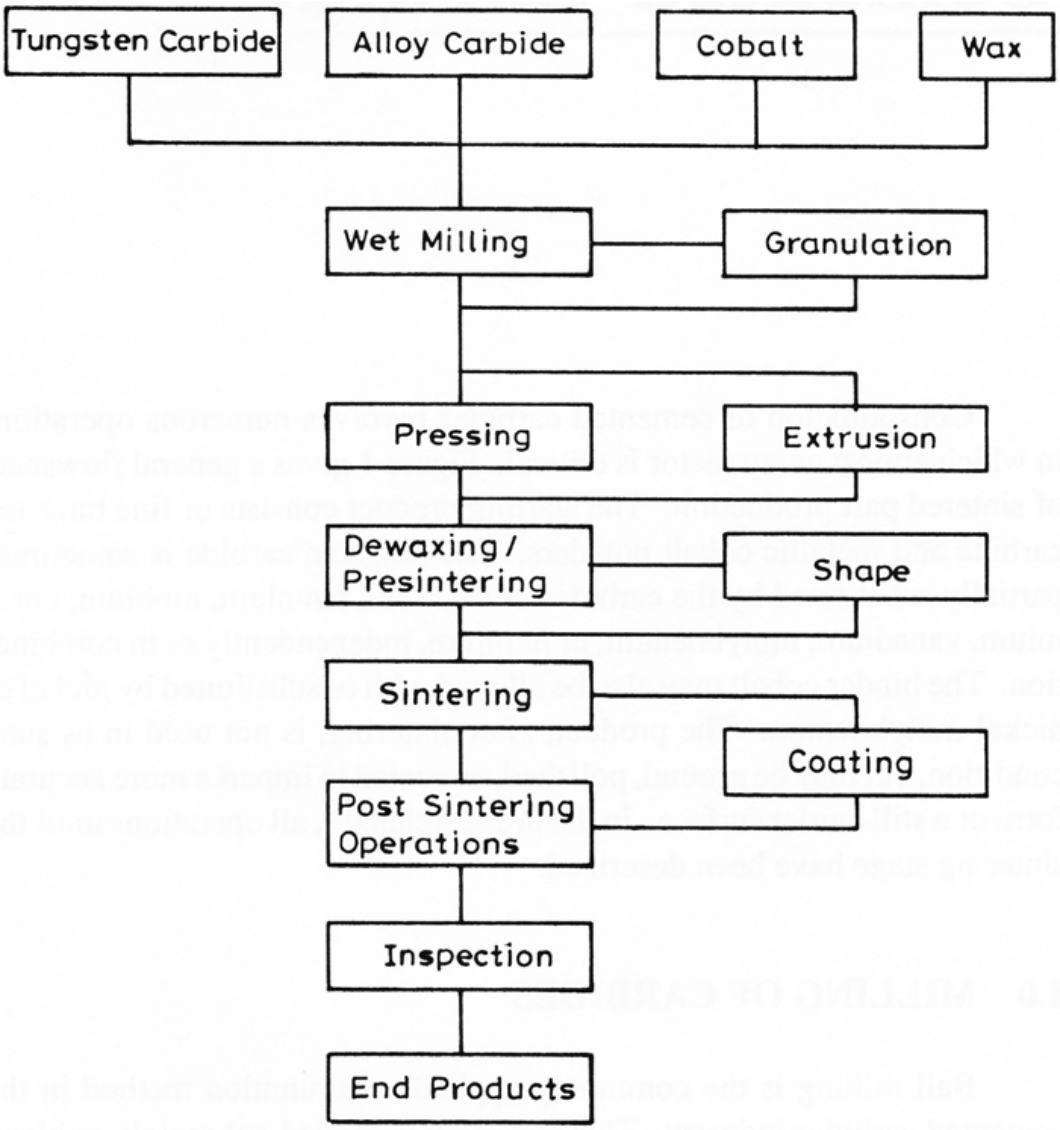

Figure 2: General flowsheet of cemented carbide production [2].

powders and decrease the grain sizes of the different powders where a longer milling time generally means a smaller grain size [2][4]. The milling process is facilitated by milling bodies of cemented carbides (cylpeps). The milled powder suspension has a low density, is difficult to fill the pressing dies with and has high inter-particle friction [2]. This makes the powder very difficult to press and sinter and it is therefore spray dried. In this process, the suspension is sprayed into a stream of 170-210 °C nitrogen [2]. This removes the milling aid from the suspension and, due to surface tension forces, creates spherical granules with the diameter 20-200 μm, each containing millions of grains [2].

Pressing

There are a couple of ways in which the material can achieve its desired shape. The most common, and the one that was used for preparation of the samples in this study, is pressing. The spray dried granules are poured into the pressing die. The granules are then pressed with a pressure in the 50-150 MPa range [2]. The pressed material, known as the green body, still retains a high porosity and has a density that is approximately 55 % of the density of the finished product. The grains in the green body are kept together by the pressing aid and the green body is therefore very brittle.

Sintering

The sintering process (Fig. 3) is a heat treatment process with the purpose to remove the pressing aid, densify the material by removal of the pores and to bind different grains to each other [4]. In the first step of the sintering, at temperatures in the range 200-300 °C, the pressing aid is removed by vaporization, a process that might be facilitated by flowing hydrogen [2]. Below the melting point of the binder phase (approximately 1300 °C), solid-state sintering occurs. In this process, chemical concentration gradients in the material causes diffusion and thereby a densification of the material [5]. The smaller the initial WC grain size is, the more of the densification occurs during solid state sintering and for materials with an average grain size below 500 nm, up to 90 % of the densification takes place during this process [6]. When the temperature is increased above the binder melting point, liquid-phase sintering starts and during this process, WC grains rearrange in the liquid binder [2]. This removes the porosity of the material and thus is the material densified. In order to have a material with a porosity low enough, a holding time of at least 30 minutes at the sintering temperature (often around 1400 °C) is generally used.

During sintering, WC grains grow due to the solution-reprecipitation process Ostwald ripening [5]. The principle behind this growth process for cemented carbide is that smaller WC grains have a higher solubility in the binder than larger WC grains. This causes a W and C gradient in the binder phase that leads to the growth of the larger WC grains. The process is believed to be interface controlled [7]. WC grain growth is also believed to be caused by grain boundary migration during the sintering process [8]. Both these processes will reduce the number of WC grains in the material thus increasing the mean WC grain size. However, a fine grained cemented carbide material is needed when the cutting application is very precise, such as drilling of small holes in a printed circuit board. Also, for a constant amount of binder phase, a fine grained cemented carbide is harder than a coarse grained [9]. On the other hand, as hardness increases, the toughness decreases [10]. In order to decrease the effect of grain growth, well known grain growth inhibitors such as Cr or V, can be added to the powder mixture [11]-[12]. During cooling of the specimen, additional solid-state sintering occurs. It should be mentioned that the binder phase still will contain a few atomic % W.

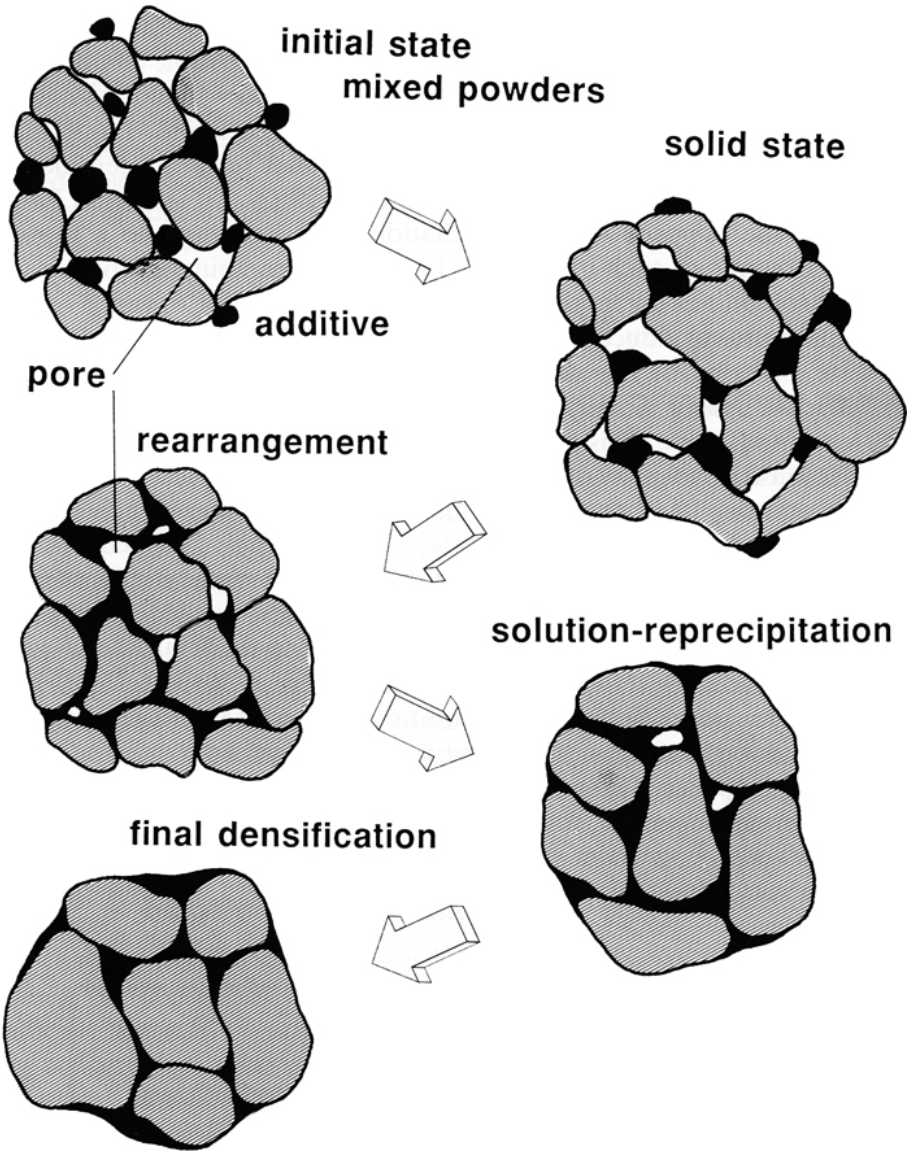

Figure 3: Schematic diagram of the sintering process [5].

Coating

Most cemented carbides are coated as this decreases the problem with a decrease in wear resistance for materials with higher toughness [4]. The coatings are either carbides, nitrides, carbonitrides, oxides or combinations of these. Two different processes are used to deposit the coating on the surface of the cemented carbide; physical vapour deposition, PVD, and chemical vapour deposition, CVD. The final coating will have a thickness between 0.5 and 20 μm.

2.3 Production control

Relative magnetic saturation to Co

It is of highest importance to control the powder mixture as a too high carbon content leads to formation of graphite and a too low carbon content leads to formation of an additional carbide phase, often designated η-phase, during sintering (Fig. 4). The presence of graphite or η-phase leads to a brittle material with no use as cutting tooling material. It is possible to get information about the carbon content in the as-sintered material by a fast and non-destructive method. The relative magnetic saturation uses the magnetic properties of Co to get information on the carbon content of the material. The higher the concentration of Co is in the binder phase, the higher the magnetic saturation is. For a certain total Co content, the measurement gives information of how much W, and other elements added to the material, that has dissolved in the binder since these elements all change the magnetic properties in the binder. This means that the WC window in the phase diagram (Fig. 4) can be related to a window in relative magnetic saturation.

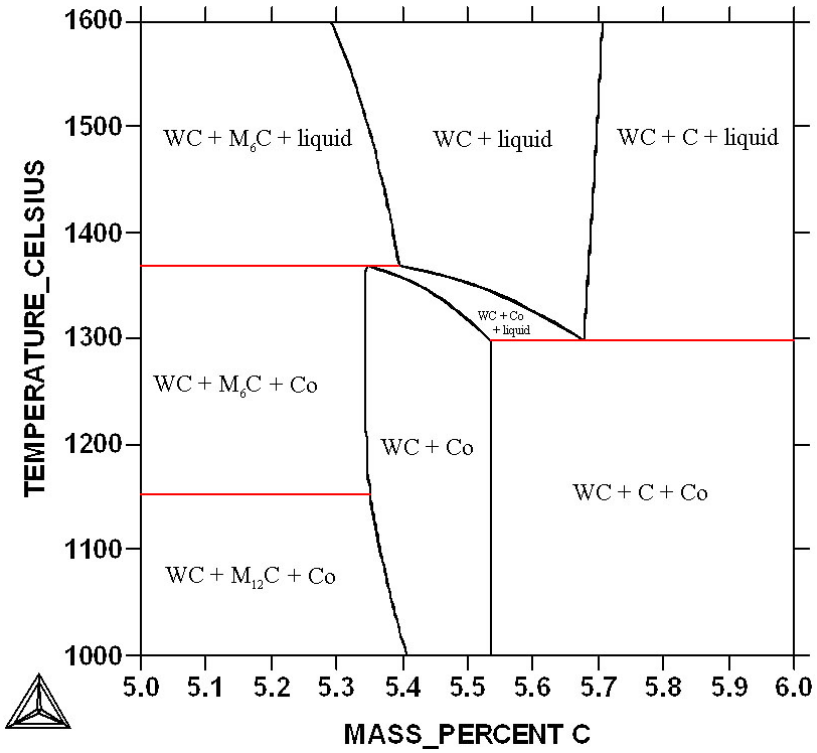

Figure 4: Phase diagram of the W-C-Co system with 10 weight % Co from the Thermo-Calc software with a database for cemented carbides developed for this class of materials [13]-[14].

Coercivity

The hardness of the material is related to the WC grain size; a more fine grained material means a material with a higher hardness. A measurement of the grain size can be achieved from coercivity measurements of the material. The coercivity depends on the size of the magnetic domains; i.e. the size of the binder volumes. For a constant amount of Co, the coercivity to the largest extent depends on the grain size of WC; a more fine grained material means a higher coercivity.

Hardness testing

Even if the coercivity gives a good approximation of the hardness, it is also desired to have a more precise testing method. One commonly used testing method for cemented carbides is the Vickers method. A pyramid of diamond is pressed into the surface of the material. The size of the impression is then related to the hardness of the material where a smaller impression means a higher hardness.

Porosity measurement

With optical microscopy it is possible to see and measure the amount of porosity, and if the production parameters not have been correct, also the amount of graphite and η-phase. The porosity is graded as AXXBYYCZZ where A means pores smaller than 10 μm, B pores with a size between 10 and 25 μm and C graphite [15]. The numbers XX, YY and ZZ are related to the amount of A, B and C defects, respectively, where A00B00C00 is the best possible material.

2.4 Microstructure

The typical microstructure of a WC-Co based cemented carbide is seen in Fig. 5. In this SEM image, WC grains appear bright and form a continuous skeleton. The binder phase, mainly consisting of Co, appears dark and is also forming a continuous skeleton for binder phase fractions mainly used in commercial products.

WC phase

The unit cell of WC is hexagonal with lattice parameters a = 0.2906 nm and c = 0.2837 nm [3]. Due to the difference in spacing between the tungsten and carbon planes in the [1010] direction, grain growth of the WC crystal causes its prismatic shape [3]. It is generally believed that the solubility of different metal atoms in WC is low [2].

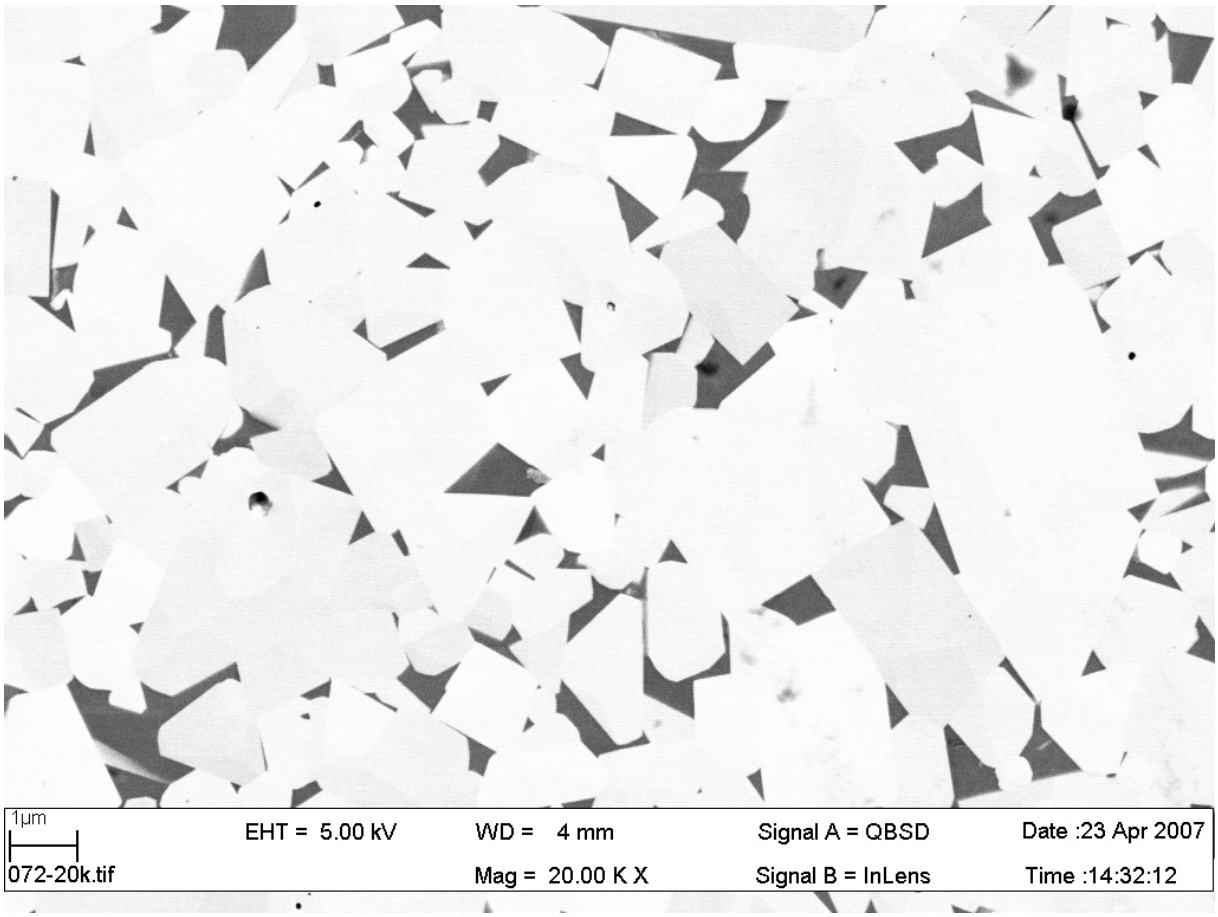

Figure 5: SEM micrograph of a WC-Co cemented carbide.

The c/a ratio for WC being almost equal to 1 (0.976) gives rise to the possible formation of coincidence site lattice (CSL) grain boundaries [16]. These have the property that if the lattice describing the atom positions at one side of the grain boundary is extended into the other one, a fraction of the lattice points will coincide. For the $\Sigma 2$ grain boundary, half of the lattice points coincide. From atomistic calculations it was shown that there exists a $\Sigma 2$ WC/WC grain boundary with lower interfacial energy than other investigated grain boundaries [17].

Binder phase

Even though it is possible to use both Fe or Ni as a binder in cemented carbides, Co is the element mainly used [2]. Co becomes liquid during the sintering and large amounts of W, C and other elements used in the production, are easily dissolved. When solidified, the binder, still with high concentrations of W and other elements substitutionally dissolved, takes the

fcc structure. The dissolved elements will make it difficult for an otherwise natural phase transformation, at 418 °C for pure Co, from fcc to hcp to occur [18]. The result will be a combination of the fcc structure with stacking faults and the hcp structure [19]. Due to difficulties in nucleation it is also seen that the Co grains are very large, up to 1 mm for some cemented carbides [20], and dendritic in their shape.

Cubic carbide phase

Cemented carbides only consisting of WC and Co will suffer from crater wear when used for cutting steel due to the carbon affinity of the steel [4]. Therefore, additions of cubic carbides such as TiC, ZrC, NbC and TaC are generally made to the powder mixture. The solubility of these metals is low not only in WC but also in the binder and therefore one or more additional cubic carbide phases are created (Fig. 6). These carbide phases help WC to build the continuous hard phase skeleton.

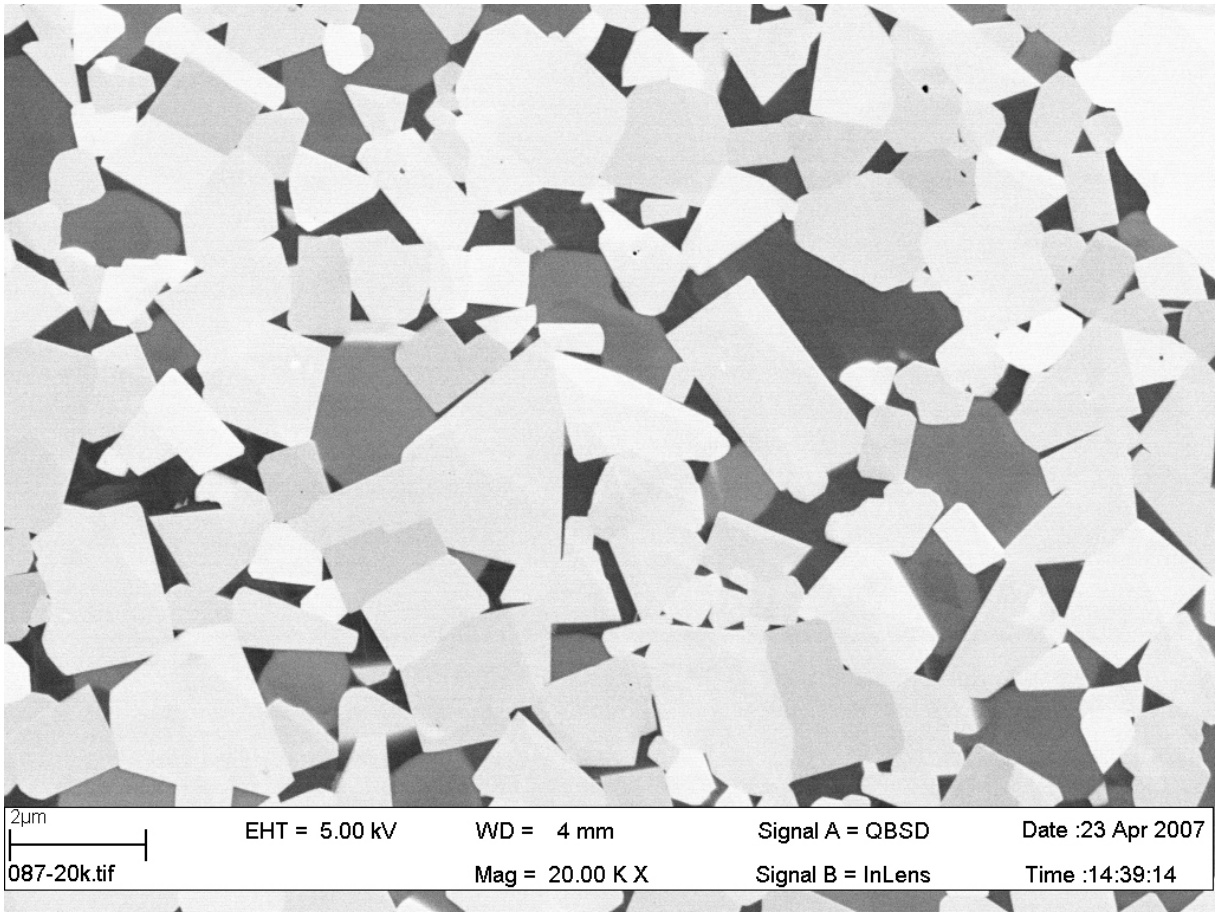

Figure 6: SEM micrograph of a WC-NbC-Co cemented carbide.

2.5 Interfaces

The analysis of interfaces in cemented carbides can give increased understanding of the grain growth and grain growth inhibition as well as the strength of the material and how it is deformed when used in metal cutting applications.

WC/binder phase boundaries

The Ostwald ripening process causes WC grain growth at the interface between the WC grain and the binder phase. As V is known to be the most effective grain growth inhibitor [11], lots of effort has been made to analyse the WC/binder phase boundaries. First with EDX in TEM, and later with high resolution TEM, it was found that V segregates to phase boundaries and there forms a thin cubic VC film [21]-[27]. It has been found that the V-rich layer is thinner for a rapidly cooled specimen [27]. Thus, it is believed that it is formed at the cooling part of the sintering process [27]. It is also believed that the grain growth inhibiting process for V involves a continuous adsorption and desorption of V atoms at the WC/binder phase boundary [27]. Studies on WC-Co based cemented carbides with Cr additions show that also Cr segregates to some WC/binder phase boundaries [28]-[29].

WC/WC grain boundaries

When used in metal cutting applications, the cemented carbide tool material may deform plastically. Some of the WC/WC grain boundaries are broken and infiltrated by a 10-50 nm binder lamella [30]. Increasing the grain boundary strength is therefore of great interest. Ab initio calculations predict that submonolayer segregation of Ti, V, Cr, Mn and Co will lower the interface energy and increase the work of separation [31]-[32]. Segregation of V [22] as well as of Cr and Co [33] has been experimentally verified.

3 Experimental techniques

When the surface of a material is to be investigated, the natural way is to use as simple methods as possible. The resolution, the smallest distinguishable distance between two closely packed objects, plays an important role. If the bare eyes do not give a resolution high enough, the assistance of a magnifying glass might do, and if this is not sufficient, the use of an optical microscope might be. Due to diffraction, the resolution (δ) is limited by the wavelength (λ) of the used light as defined by the Rayleigh criterion [34] as equation (1).

$$\delta = 0.61 \times \lambda \tag{1}$$

Visible light has a wavelength in the region 400-800 nm and it is therefore impossible to get a better resolution than around 250 nm with optical microscopy. Since cemented carbides often have a mean WC grain size smaller than 1 μm, optical microscopy does not have sufficient resolution and is therefore unsuited for investigation of the material. Also, optical microscopy cannot give information such as the chemistry or the crystallography of the material.

3.1 Electron microscopy

The foundation for electron microscopy is based on the idea from Louis de Broglie that a particle also has wave properties [34]. The particle wavelength λ is related to the particle momentum p and Planck's constant h as equation (2).

$$\lambda = \frac{h}{p} \tag{2}$$

Electrons with charge e that are accelerated by a potential V will get the kinetic energy $E_k = eV$. Combined with equation (2) and expressing the electron rest mass as m_0, this gives the electron non-relativistic wavelength λ as equation (3).

$$\lambda = \frac{h}{(2m_0eV)^{1/2}} \tag{3}$$

With $e = 1.602\times10^{-19}$ C, $m_0 = 9.109\times10^{-31}$ kg and $h = 6.626\times10^{-34}$ Nms, equation (3) gives that a voltage above 1.51 V is enough for an electron wavelength shorter than 1 nm.

Electron gun

In all electron microscopes, the generation of electrons takes place in the gun. Older microscopes use thermionic guns where electrons are generated by heating of either a hairpin-shaped tungsten wire or a tiny block of single-crystal lanthanum hexaboride (LaB_6). The heating causes the electrons to exceed the energy barrier at the surface and therefore escape into the vacuum. A Wehnelt cylinder is located around the emitter with the purpose to focus the electron beam and control the amount of electron emission. The last part of the thermionic gun is the ground potential anode, which attracts the electrons from the highly negative emitter. A small hole in the anode allows electrons to pass down through the microscope column.

Newer microscopes use a field emission gun (FEG). The emitter in the FEG consists of a sharp tip of tungsten connected to a negative potential. The electric field concentrates on the tip and when it is in the order of 10 V/nm [34], electrons tunnel through the potential barrier of the tip. Two anodes are located below the emitter. The first anode provides the extraction voltage. It is positively charged by about 2-4 kV relative to the tip and has the purpose to help the electrons to tunnel from the tip [34]. The second anode accelerates the electrons to the desired energy.

The advantage with a FEG is that it has a higher brightness, a smaller energy spread and a smaller crossover than a thermionic gun. On the other hand is it much more expensive and requires a better vacuum.

Electron lenses

Most lenses in electron microscopes are electromagnetic [34]-[35]. An electromagnetic lens consists of a coil of copper wire surrounded by a shielding case of soft iron. On the inside of the core there is a gap in the iron, that gives room to the polepieces, which are made of soft iron as well. It is here that the refraction is taking place due to the fact that a current running through the copper windings will give rise to a magnetic field. The field is formed by the polepieces. Since the electrons are charged particles, the magnetic field will affect the electrons by a force known as the Lorentz force, being proportional to the strength of the magnetic field. Since the strength of a magnetic field is inversely proportional to the distance from the source and due to symmetry reasons, the lens will work as desired. By changing the current through the windings, the strength of the lens can easily be adjusted. Often, stigmators are located close to the lenses. The stigmator corrects for astigmatism, the aberration were two perpendicular planes of incoming rays do not cut each other in a focal point but along two focal lines. A stigmator applies a weak magnetic field to make the lens symmetric to the electron beam by using an octupole with four sets of opposing magnetic poles [34].

3.2 Scanning electron microscope (SEM)

In the top of a scanning electron microscope (SEM), electrons are generated by an electron gun, and are accelerated to somewhere up to 40 keV (Fig. 7). The electrons enter the lens system that consists of a number of (first) condenser lenses and (second) objective lenses. The condenser lenses demagnify the crossover of the electron beam, thereby reducing the spot size. The objective lenses control the focus of the image, i.e. focus the electron probe onto the specimen surface.

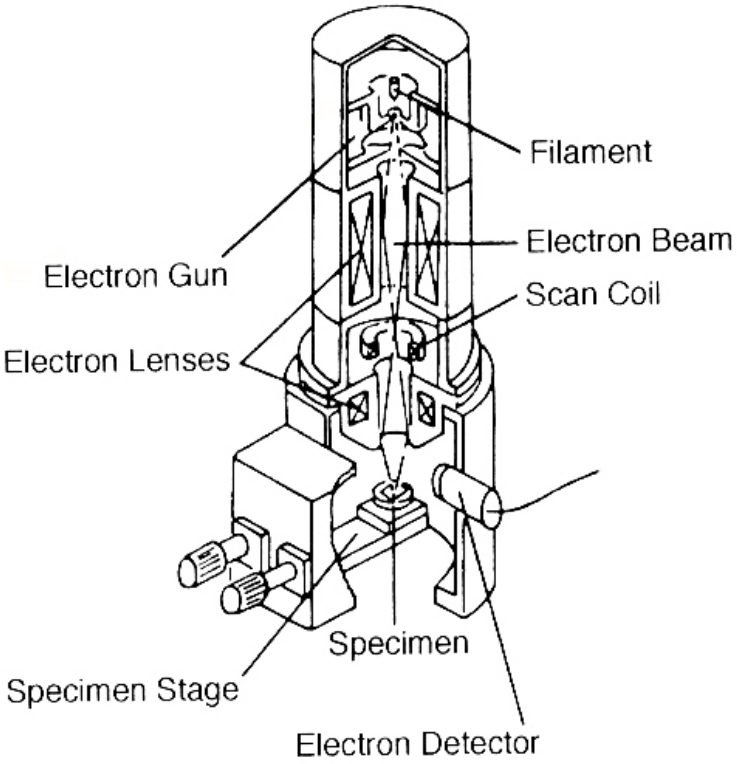

Figure 7: Microscope column of a SEM [35].

The scanning procedure in a SEM is performed by the scanning coils located between the condenser and the objective lenses. The scan over the specimen surface is synchronized with the scan on a computer screen, which means that an image of the object can be displayed. The magnification in the image is given by the ratio between the width of the computer screen and the width of the scanned specimen area.

When the incident beam of high-energy electrons hits the specimen, loosely bound electrons from the specimen are knocked out, i.e. secondary electrons (SE). Most of the SE come from a volume near the surface, the extent of their interaction volume is in the order of 1-10 nm, and they have energies between 0 and 10 eV [35]. The most common detector

for SE is the Everhart-Thornley (ET) detector. It consists of a collector and a scintillator, both positively biased in order to catch as many low energy electrons as possible. The photons, created by the electrons hitting the scintillator, are sent through a light pipe and then retransformed into electrons that are further amplified. The signal is then sent to the computer screen.

At the interaction with the surface, some of the high-energy incident electrons will scatter against the specimen in such a way that they will leave the specimen. The interaction volume of these backscattered electrons (BSE) is up to 1μm and they have energies up to the energies of the incident electrons. The BSE can be detected by a negatively biased E-T detector, thus repelling the low energy SE, or a detector with a scintillator not sensitive for low energy electrons [35].

As a rule of thumb, SE give better resolution and are therefore mainly used when the topography is to be analysed. The generation of BSE depend on the atomic number of the specimen and BSE are therefore suitable for separation of different phases such as imaging of the surface of a polished cemented carbide material.

3.3 Electron backscatter diffraction (EBSD)

An electron backscatter diffraction (EBSD) system is an add-on for the SEM that can give information about the phase and crystallographic orientation of the investigated specimen (Fig. 8). Some of the electrons that hit a specimen will be inelastically scattered in such a way that they will fulfill the Bragg law, given in equation (4). Here d is the distance between the atomic planes in the material, θ is the angle between the electron beam and the atomic planes, m is a positive integer and λ is the wavelength of the electrons.

$$2dsin\theta = m\lambda \tag{4}$$

If the surface of a crystalline specimen is well polished and if the signal-to-noise ratio is high enough, it is possible to detect an electron backscatter pattern (EBSP) of the backscattered electrons on a thin fluorescent screen. A CCD camera positioned behind the screen takes a picture of the pattern and send it to the computer for further analysis (Fig. 9). The computer then transforms the image to the crystal structure and orientation at the point of analysis. If this procedure is repeated at grid points over a large area, it is possible to make a reconstruction of surface properties of interest such as the orientation of the grains (Fig. 10) or the appearance of special grain boundaries (Fig. 11). It will also be possible to make quantitative measurements of such parameters as the grain size or the fraction of special grain boundaries for a polycrystalline material.

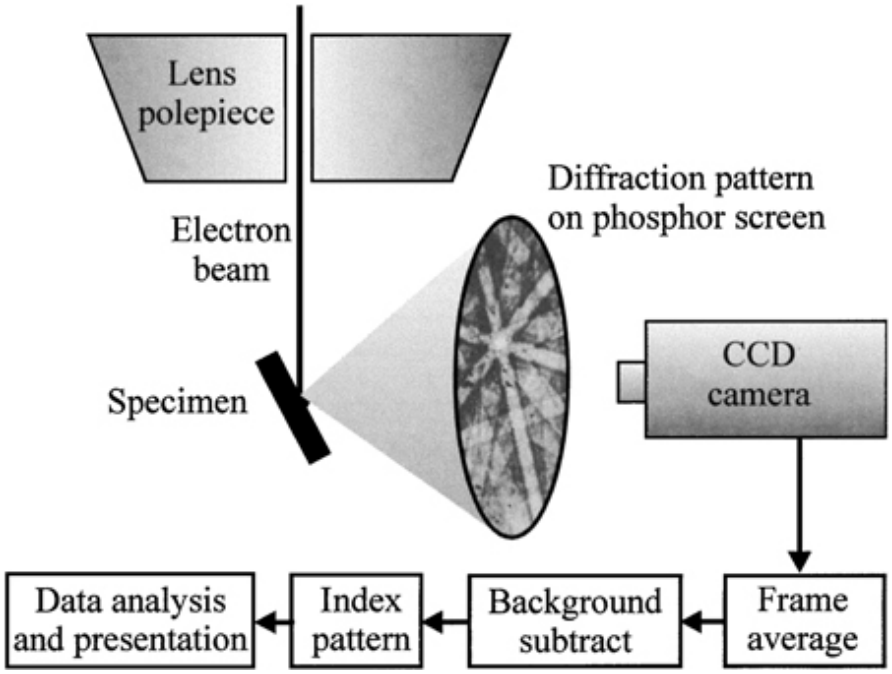

Figure 8: Principle of the EBSD technique [36].

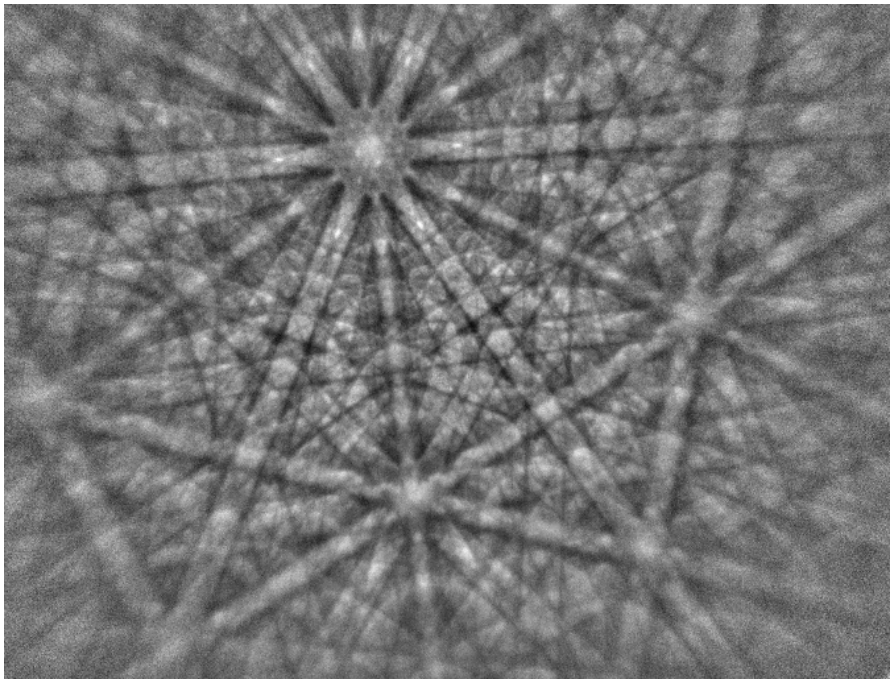

Figure 9: EBSP of a WC grain.

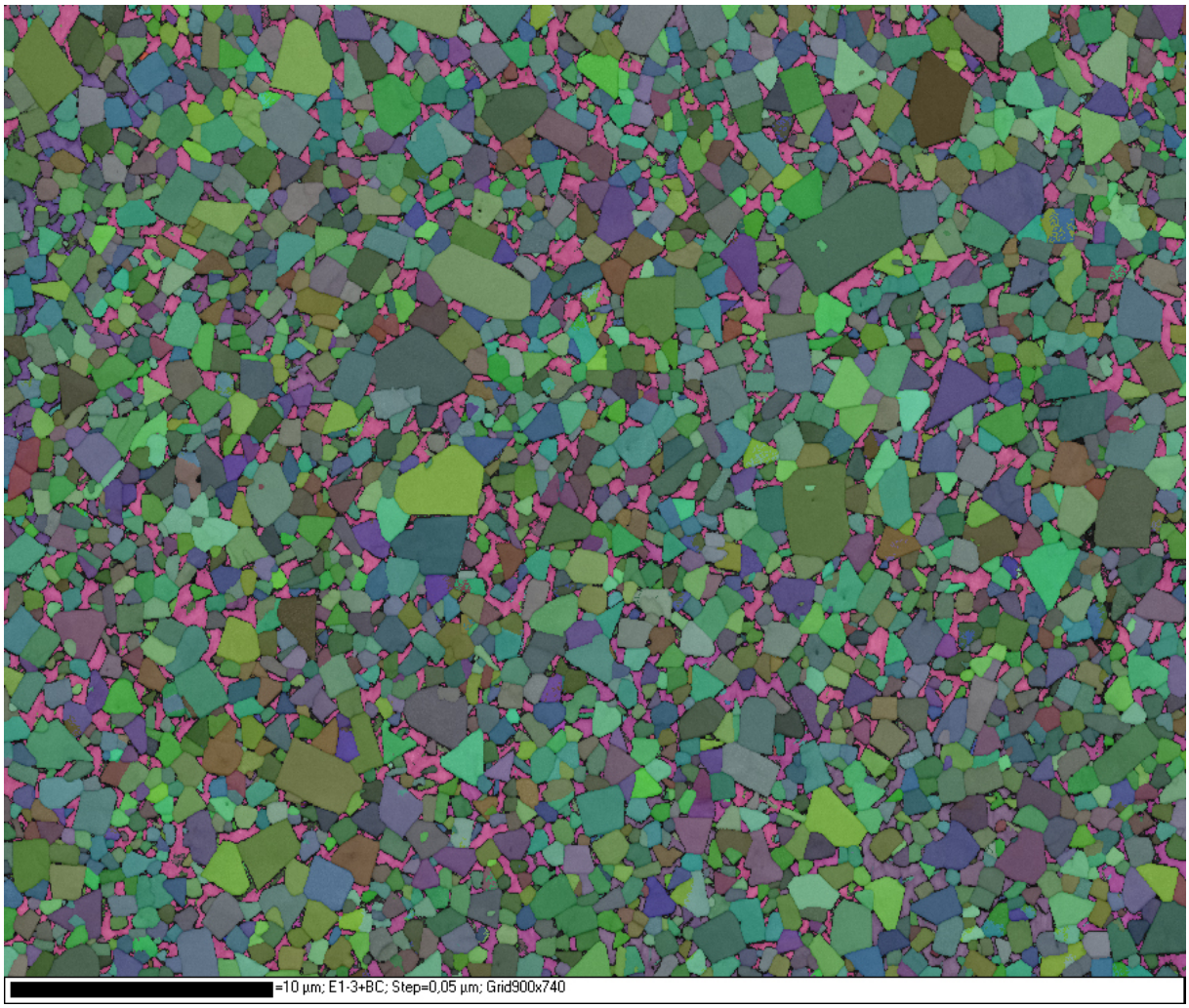

Figure 10: EBSD reconstruction of a WC-Co cemented carbide. Each colour represents a certain orientation of a WC or a binder phase grain.

3.4 Focused ion beam (FIB)

Closely related to the SEM is the focused ion beam (FIB) workstation. The difference is that instead of electrons, Ga^+ ions are now being used. One advantage with the use of ions is that the higher momentum of these enables local milling. The disadvantage is that the higher mass of the particles causes a risk of unintended radiation damage, or even destruction of the specimen surface. Most FIB workstations include one or several gas systems that can be used for depositing of a protecting layer on the specimen surface or, as will be explained in the specimen preparation section, for micro-manipulation in the analysis chamber.

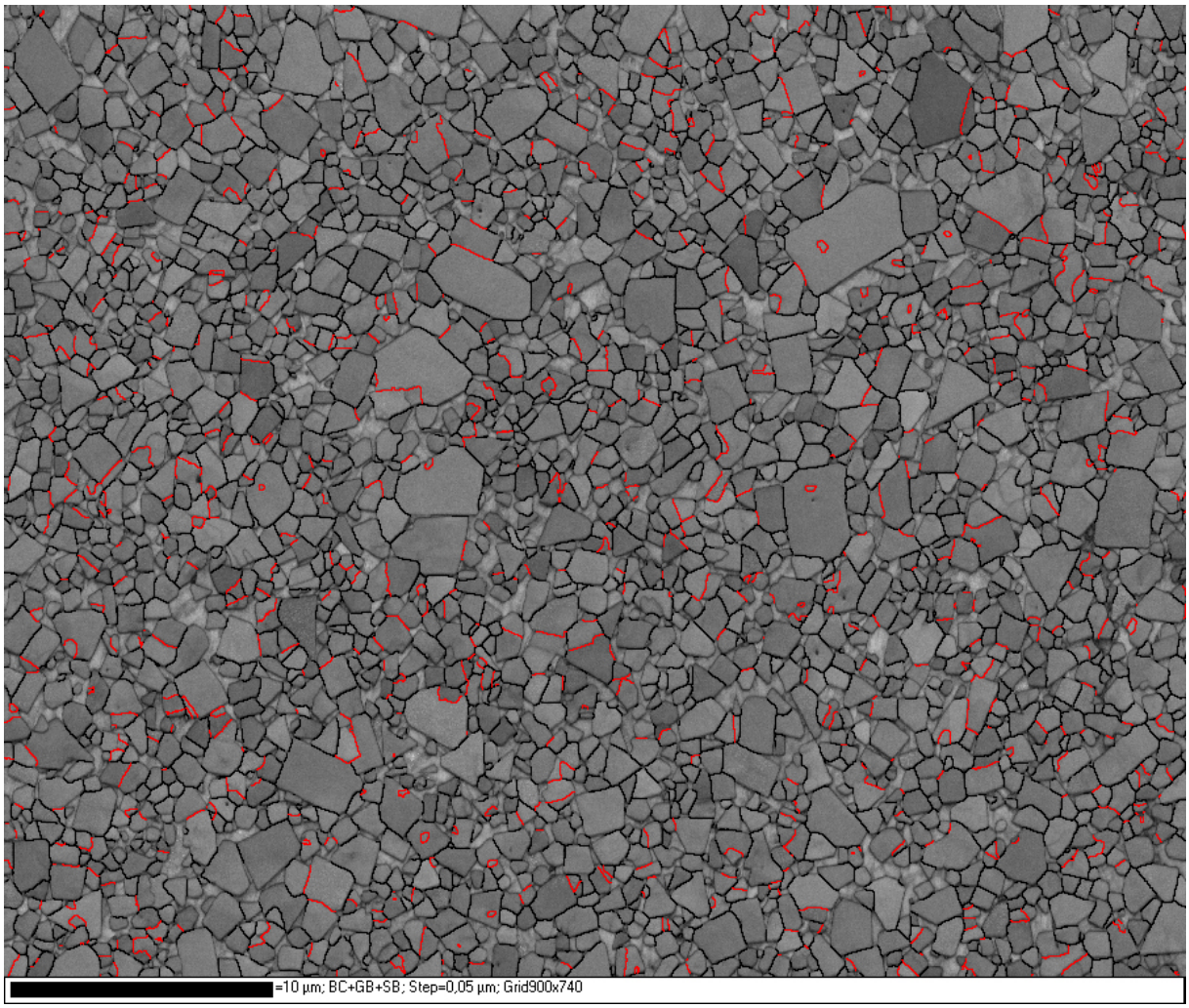

Figure 11: EBSD reconstruction of the same WC-Co cemented carbide as in Fig. 10. The greyscale shows the band contrast that gives a measurement of the quality of the EBSP. Red lines show Σ2 WC/WC grain boundaries and black lines show other, random, WC/WC grain boundaries with a misorientation larger than 10°.

The Ga^+ ions used in the FIB come from a liquid metal ion source (LMIS). The LMIS consists of a tungsten needle, shaped in a conical form with a reservoir of liquid gallium placed on the top. Gallium is chosen as field emitter since it is a liquid at room temperature, can give high brightness and has a small emission area [37]. By applying a sufficiently high electric field to the tip, the liquid will be under stress and form a "Taylor cone" [38]. Now ions can break the potential barrier and then approach the sample through the ion column [37].

3.5 Transmission electron microscope (TEM)

A specimen with a thickness below 100 nm will be transparent to high-energy electrons, a phenomenon used in transmission electron microscope (TEM) where the acceleration voltage most often is in the range 80 to 400 kV. The TEM consists of an illumination system, an image forming system and a projection system. The obtained image can either be displayed on a fluorescent screen or be photographed by a camera (Fig. 12).

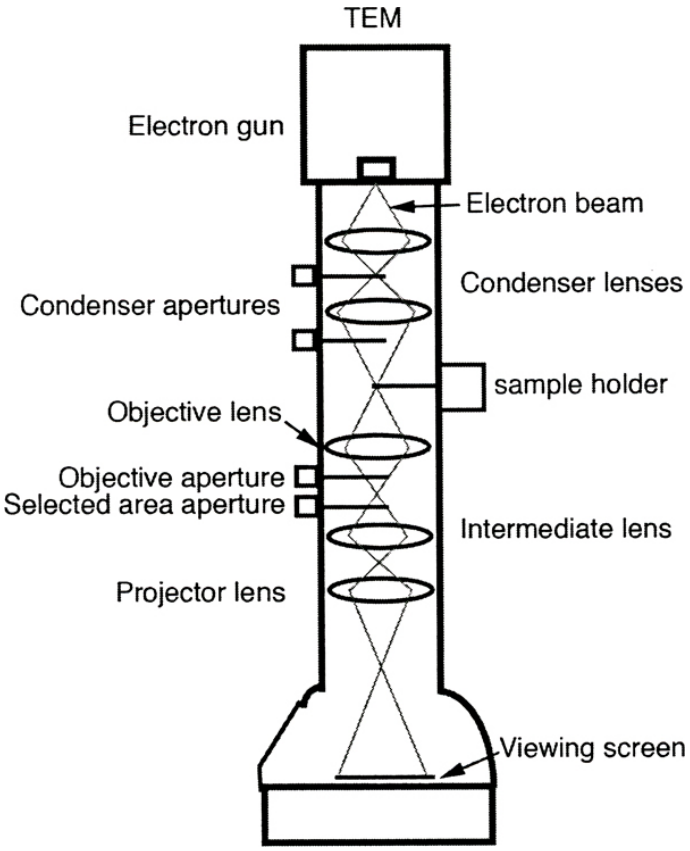

Figure 12: Principle of a TEM [39].

Illumination system

The illumination system consists of an electron gun and a condenser system. The condenser system usually consists of two or three lenses with one aperture for each of them. For a two-lens system, the first condenser lens is the stronger one with a magnification in the order of 50× which means that it demagifies the beam crossover with the same ratio and thereby determines the spotsize [34]. The first condenser aperture limits the beam load on the specimen. The second condenser lens is weaker and has the purpose to determine

the size of the illuminated area and project the demagnified image on the specimen. The second condenser aperture determines the beam divergence. Using a three-lens system, it becomes easier to have parallel illumination of the specimen [40].

Image forming system

The objective lens changes the focus and determines the resolving power of the microscope. Since it is the first lens in the image forming system, and aberrations therefore will be magnified in the projection system, it is of greatest importance that it is as well constructed as possible. The size of the objective aperture controls the contrast of the image. If the aperture allows the direct beam to reach the image plane, a bright field image is obtained. If a diffracted beam is allowed, a dark field image is obtained.

Projection system

The lenses between the objective lens and the screen, the diffraction lens, the intermediate lens and the projector lens, all have the purpose to magnify the image. The lenses can also be used to switch between image mode and diffraction mode (Fig. 13). The selected area aperture is used to select the area of the specimen from which the diffraction pattern is formed.

3.6 Energy dispersive X-ray spectroscopy (EDX)

Energy dispersive X-ray spectroscopy (EDX, or sometimes called EDS) is a an add-on for analytical microscopy in both SEM and TEM. When the incident electron beam hits an atom in the specimen, it might cause an inner shell electron to be emitted, thus resulting in an excited atom. An electron from an outer shell then almost immediately jumps to a inner shell and the energy difference is sent out as an X-ray, characteristic for the element that was excited. The X-rays can be detected by a Si(Li) crystal where a electron-hole pair is created for every 3.86 eV of the X-ray [35]. The pulses are then stored in a multichannel analyser where each channel represents a certain amplitude interval of the pulses. Apart from the element characteristic energies in an energy spectrum an exponentially decreasing background known as bremsstrahlung (or ”braking radiation”) can also be seen, originating from acceleration of the incident electrons in the field of the nucleus [35].

For TEM, the spatial resolution of an EDX-analysis can be nearly as good as the size of the spot, i.e. a couple of nm [34]. For SEM on the other hand, due to scattering, X-rays can be generated at distances in the order of μm away without any problems leaving the specimen and thereby causing the resolution limit to be of this order [35]. An EDX system has the advantage of being fast and easy to use. On the other hand, it has poor energy resolution

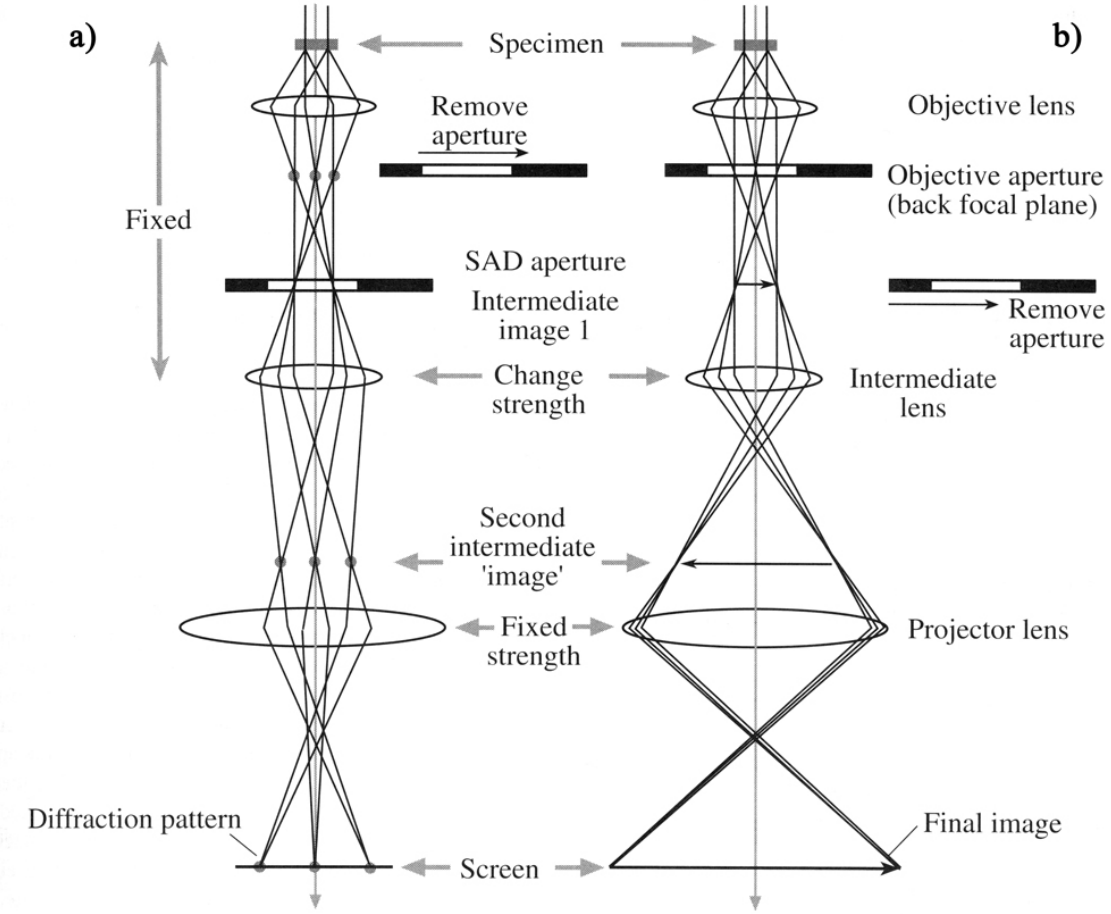

Figure 13: Ray diagrams in TEM for (a) diffraction mode and (b) imaging mode [34].

(100-150 eV [34]), low sensitivity for lighter elements and limitations in detection of very small concentrations and fine level accuracy. The problems with analysing lighter elements is due to absorption of their low-energy photons in the specimen and in the window to the detector, as well as due to the low energy resolution causing difficulties in separating energies for lighter elements as these are closer than for heavier elements.

3.7 Atom probe tomography (APT)

The limitations of EDX gives need for the use of atom probe tomography (APT). The instrument analyses specimens shaped as sharp needles with a hemispherical tip with a radius below 100 nm. A positive DC voltage of 1-15 kV is applied on the specimen. Traditionally (Fig. 14), a counter electrode is positioned a couple of mm away and short negative pulses with the magnitude approximately 20% of the DC voltage are sent to the counter

electrode. The electric field will be highest at the tip of the specimen and if high enough, field evaporation, an ionisation of the surface atoms, will occur [41]. This happens when the ionic state of the atom has a lower energy than the atom state. The field needed for field evaporation differs with element and crystallographic orientation. If the field is high enough, it is possible to get multiple ionisations. In practice, light elements such as C will be predominately field evaporated as singly or doubly charged ions and heavy elements such as W will be predominately field evaporated as triply or quadruply charged ions. As the field evaporation process progresses, the specimen will become more and more blunt and thus, the voltage has to be increased. The electric field will give rise to a mechanical stress on the specimen that sooner or later will cause a specimen fracture. Modern APT instruments therefore has the option of using laser pulsing, thus having a thermal activation, instead of voltage pulsing [42] and thereby decreasing the mechanical stress. Some instruments has also decreased the distance between the specimen and the counter electrode (local electrode) in order to detect ions from higher angles, i.e. from a larger part of the tip surface [42].

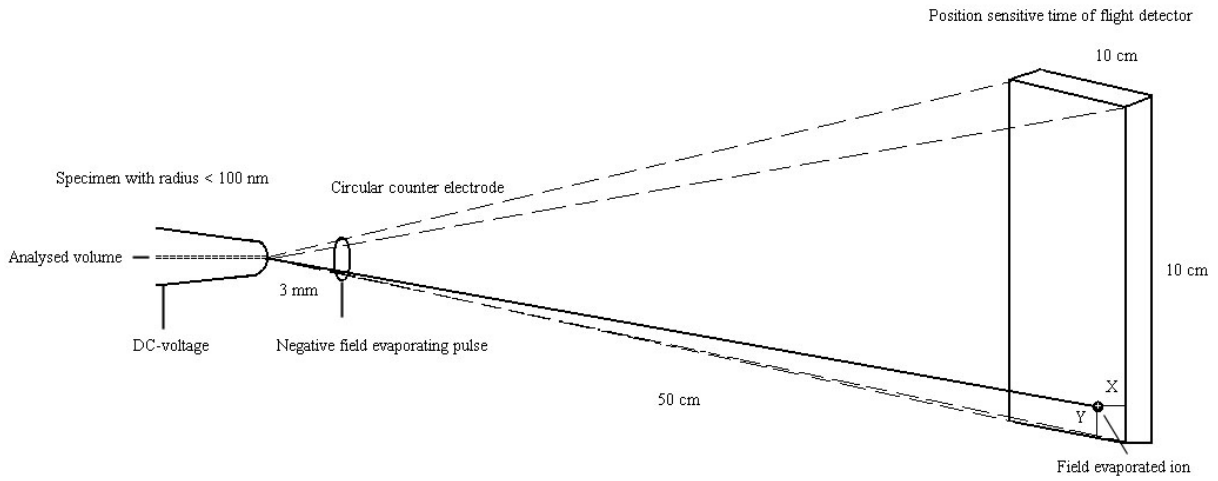

Figure 14: Schematic view of APT.

In some APT instruments, the ions will pass through a reflectron lens working as an energy compensator where ions with higher energy will travel a longer distance. In this way, the mass resolution will not be affected by the possibility of field evaporation when the voltage pulse has decayed somewhat. Finally, the ion will hit a position sensitive detector and at the impact, clocks started at the pulse signal will be stopped. The kinetic energy at the impact with the detector can be approximated to be equal to the potential energy, eV, just before field evaporation. By neglecting the time for acceleration, it is possible to relate the time of flight, t, the distance between the specimen and the detector, d, and the specimen voltage, V, to the mass over charge, m/n, of the ion as equation (5).

$$\frac{m}{n} = 2eV\frac{t^2}{d^2} \tag{5}$$

The position in the evaporation sequence, the time of flight, the voltage and the hit position on the detector is recorded for every detected ion by a computer. The times of flight are recalculated to atom masses over charge and inserted in a spectrum (Fig. 15). The peaks in the spectrum are defined as different elements and each of these elements are given a specific colour. Using the recorded data it is then possible to create a reconstruction of the specimen where a single detected ion is represented by a dot (Fig. 16).

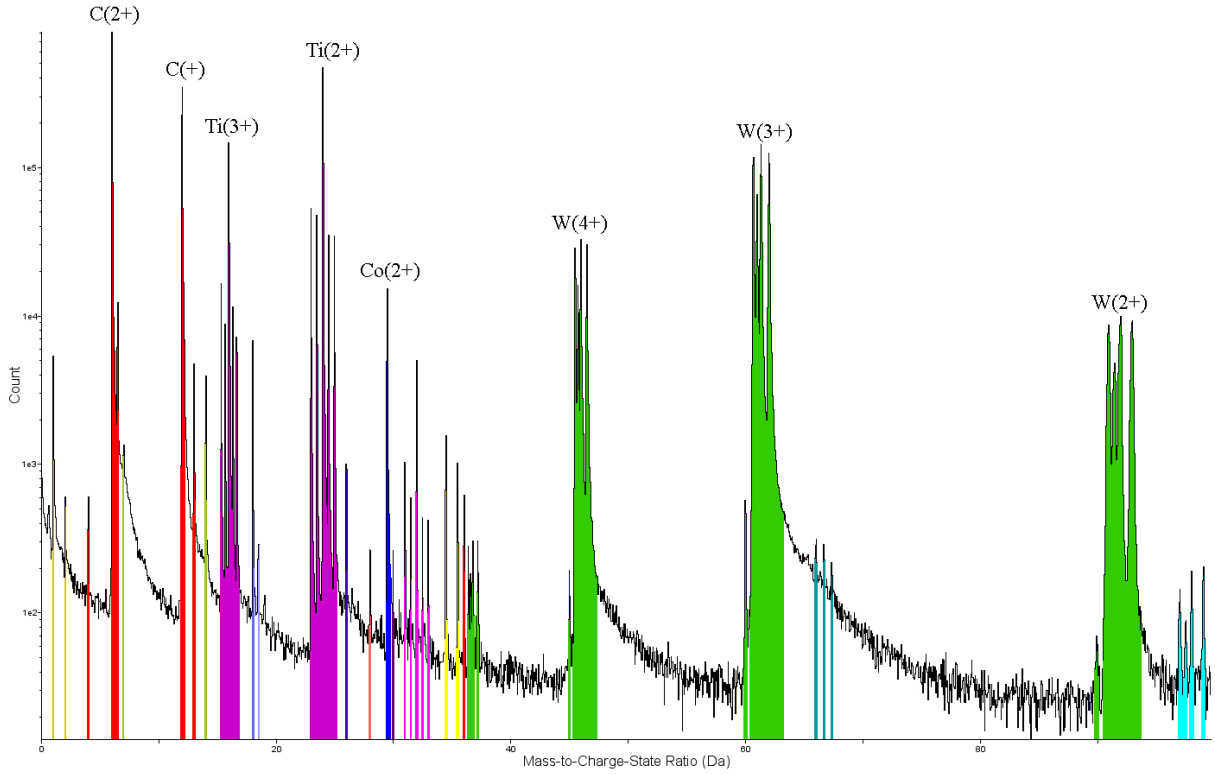

Figure 15: Mass to charge spectrum of an APT analysis of a WC-TiC-Co cemented carbide. The largest peaks are labeled in the image.

APT cannot detect all of the field evaporated ions. In older APT instruments, the counter electrode was placed a couple of mm away from the specimen. As the ions then will leave the specimen surface with a trajectory perpendicular to the surface, only ions from the center of the hemisphere at top of the specimen will be possible to analyse [41]. Newer instruments uses a local electrode, placed only around 30 μm away from the specimen surface and has a smaller distance between the specimen and the detector, thereby increasing the collection angle [42]. Not even all of the ions that hit the detector will be analysed. The construction

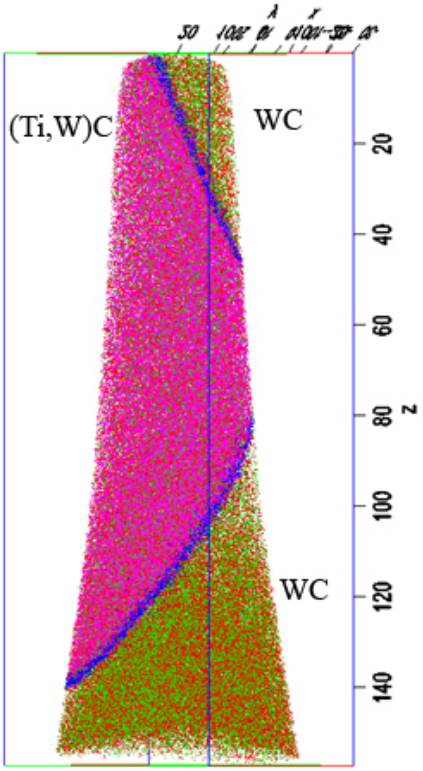

Figure 16: APT reconstruction (largest diameter 55 nm, length 148 nm) of a specimen with two WC/(Ti,W)C phase boundaries in a WC-TiC-Co cemented carbide. Green dots = W atoms, red = C, blue = Co, pink = Ti.

of the detector means that only 35-45 % of the ions will be analysed. Also, if several atoms with the same mass, separated only by a small distance from each other on the specimen surface, are field evaporated during the same pulse, there is a risk that the detector will interpret them as only one atom and thereby information is lost. In addition, a too low pulse fraction, or a too high specimen temperature, during analysis might cause a preferential field evaporation of some elements between the pulses [41]. Therefore, it is of big importance to choose good parameters during analysis and do the reconstruction carefully.

3.8 Field ion microscopy (FIM)

A technique related to APT is field ion microscopy (FIM). A gas (”image gas”), such as helium or neon, is introduced into the instrument. The specimen is faced towards a fluorescent screen and by applying a positive DC voltage to the specimen, the atoms of the

image gas will be ionised close to protruding atoms of the tip surface and hit the screen. It might then be possible to get crystallographic information about the material from the FIM image [41]. If the area of interest is a grain boundary parallel with the specimen axis, it is a big risk of missing it in an APT analysis. Since FIM gives a less magnified image of the specimen than what will be detected for APT, it might be possible to perform FIM before APT, locate the grain boundary in the FIM image and if the instrument enables specimen movement, then tilt the specimen in such a way that the grain boundary faces the APT detector.

4 Specimen preparation and experimental setup

For the work presented in this thesis, two series of materials were produced. The first series of materials, produced by Sandvik Tooling AB, consisted of one WC-Co reference material and three materials with V, Cr or Mn additions corresponding to 0.5 atomic %. The materials were designed to contain 16 volume % binder phase as-sintered. The milling time was 45.5 hours and the sintering was performed for 1 h at 1410 °C. The second series, produced by Seco Tools AB, consisted of one WC-Co reference material, four materials with TiC, ZrC, NbC or TaC additions and one material with both TiC and ZrC additions. These materials were designed to have 10 volume % binder phase and, for the materials with additions, 20 volume % cubic carbide phase as-sintered. In the material with both TiC and ZrC additions, these were added so that the amount of Ti and Zr atoms were equal. The reason for the production of this material is that the difference in lattice parameter for the cubic carbides involved causes a separation into two different cubic carbide phases. For this series, the milling time was 40 h and the sintering was performed for 1 h at 1430 °C. For both series, thermodynamic calculations were performed in order to make sure that the carbon potential was equal for all materials and far away from creation of graphite or η-phase. All materials were produced as inserts in the SNUN120408 shape (12.7 × 12.7 × 4.76 mm) in order to facilitate further specimen production.

4.1 EBSD specimen production

From the insert, a 300 μm thick slice was cut. This slice was polished with 9 and 1 μm diamond slurry, 20 minutes each. To better fit the equipment, the specimen was cut to a 5 × 4 mm piece. The outer surface layers were removed with sputtering of Ar^+ ions in a Gatan precision polishing system (PIPS) model 691. This was done in order to minimize the strain in the specimen and further increase the surface quality [17]. The energy was 4 kV, the incident angle 2° and both guns were used for two hours of sputtering.

4.2 EBSD parameters

For all EBSD work, a Leo Ultra 55 FEG SEM was used with an EBSD system manufactured by HKL and their software Channel 5. In order to get a good signal, the specimen was tilted 70°, the voltage was 20 kV and the high current mode was used.

For the first series of materials, it is fairly easy to separate between the three possible phases, WC and cubic and hexagonal Co, as these will give rise to easily separated EBSPs. For this reason, a 60 μm aperture was used in the SEM in order to get a good resolution and high signal, the detector was inserted as far as possible in order to get an as large space angle as possible and the working distance, the distance between the specimen and

the objective lens in the SEM, was set to 15 mm in order to get the center of the EBSP at the center of the camera. During analysis, the system tried to identify 6 to 8 bands. Fewer bands would lead to more indexing of pseudo symmetry and more would lead to a situation where fitting would be too poor. For the same reason, the computer was programmed to search for the 41 theoretically strongest bands. A 4 $\times$ 4 binning was used since a lower binning would slow down the collection of data too much and a higher binning would not be beneficial in time since the limiting part still would be the computer. No frame averaging was performed as this would slow down the collection of data too much and thereby increase drift problems. Also, the pattern quality was so good that there was no actual need for averaging. The Hough space level was set to 50. This transformel transforms bands to points that the computer uses to identify the crystallographic properties of the indexed pixels.

For the second series of materials, the system now had an additional phase, a face centered cubic carbide phase, to separate data into. Unfortunately, what is separating the EBSP of two face centered cubic phases with the same orientation is only the width of the bands. Standard procedure for EBSD analysis only uses the relative orientation of the bands. However, the use of the time consuming advanced fitting mode enables separation with respect to the band width. The difference in lattice parameter between Co (0.357 nm) and for the cubic carbides (0.433 nm for TiC, 0.469 nm for ZrC, 0.447 nm for NbC and 0.446 nm for TaC [18]) is enough for phase separation in this mode if smaller adjustments in the experiment setup are made. The camera is moved 7 mm away from the maximum insertion position in order to increase the magnification of the bands. The binning is changed to 2$\times$2 in order to increase the resolution. These adjustments will decrease the signal and therefore a larger objective aperture, 120 μm, should be used. The higher magnification means that there is a risk of missing some of the theoretically strongest bands and thus, the computer should now search for 6 to 9 out of the 77 theoretically strongest bands. For the material with both TiC and ZrC added, the difference in lattice parameter was so small that not even the advanced fitting mode could separate between the phases. Instead, an EDX analysis was performed simultaneously as the EBSD analysis and every cubic carbide grain was manually indexed for the evaluation of data.

Data was generally filtered for wild spikes and noise reduction. Wild spikes filtering means that if all eight neighbouring pixels of an indexed pixel are identified as the same phase and orientation, but differenting from the center pixel, the center pixel is assumed to be misindexed and will therefore copy the information from the neighbours. Noise reduction means that if a pixel lacks crystallographic information but the neighbours of the pixel are indexed as the same phase and orientation, the pixel will copy the information from their neighbours. The level of the noise reduction is a measurement on how many of the neighbours that need to have the same orientation where level 8 then corresponds to a demand for all eight neighbours to have the same information. For grain size measurements, the noise reduction level 5 was chosen to be appropriate. In order to define a grain, a minimum of three pixels was demanded in order to decrease the effect of misindexed grains

in the grain size statistics. For the detection of WC/WC Σ2 grain boundaries, the Brandon criterion [43] was used meaning that up to a 10.6° deviance from the 90° rotation around the $[10\bar{1}0]$ axis was defined as a Σ2 boundary.

4.3 TEM specimen production

In this work, the lift-out technique was used to produce TEM specimens as it is a fast and reliable method where the location of the specimen also can be chosen [44]. A FEI Strata DB 235 DualBeam workstation (DualBeam) was used and this instrument combines a SEM and a FIB with a 52° tilt between the two columns (Fig. 17). This means that when work is carried out on a specimen using ions, it is possible to image it from another angle with electrons. Having two beams also makes it easier to get the three-dimensional structure of the material.

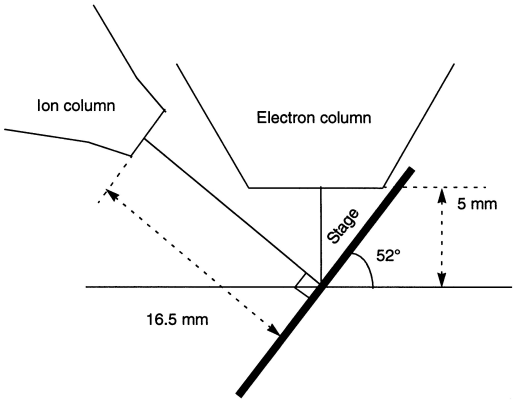

Figure 17: Schematic view of a DualBeam workstation [45].

The DualBeam has a couple of gas injection systems (GIS) that can be used to deposit a protective layer on the specimen to be investigated. By heating the GIS and then scan the surface of the specimen with the ions, the layer will start to grow. In this work, only the platinum GIS was used with the current 4×A pA where A was the deposited area measured in μm^2. For the deposition, a predefined material file, pt_mag.mtr was used, which is the standard Pt deposition file with an overlap of 50 %, a dwell of 0.2 ms and a sputter rate of 0.5 μm^3/nC.

The starting material was the specimens used for EBSD analysis as these had well polished surfaces. The specimen was first put in the DualBeam that was tilted 52°. A 30×5×2 μm protective Pt layer was deposited on the surface (Fig. 18 a). It is from below this Pt strip the TEM specimen is going to be taken. Using a current of 20 nA, two stepped holes were milled out with the deepest parts being next to the platinum strip. The upper hole had the dimensions 35×12×10 μm and the lower 35×7×20 μm. For both these holes, the predefined

material file si.mtr was used which is the standard milling file with an overlap of 50 %, a dwell of 1.0 ms and a sputter rate of 0.15 μm^3/nC. A third hole with the dimensions 7×3×20 μm was now milled to the left of the original hole (Fig. 18 b). The specimen was tilted back, now facing the electron column, and the scan rotation was changed 180° making it possible to mill from the upper stepped hole to the lower one. Such a hole was milled with the dimensions 25×3×25 μm. Simultaneously, a hole with the dimensions 3×5×25 μm was created overlapping at the right hand side of the before mentioned hole. This means that an approximately 30 μm long and 6 μm thick wedge-shaped TEM specimen was created, connected to the larger piece only by a thin strip at its right part.

The specimen was tilted 52° and then lowered. A thin needle called Omniprobe was approached to and aligned at the center of the image. The specimen was slowly raised (Fig. 18 c) until it finally touched the needle. With the Pt GIS, the Omniprobe was welded together with the specimen (Fig. 18 d). By milling away the supporting connection between the specimen and the surrounding material, the surrounding material could now be lowered (Fig. 18 e) and the vacuum chamber could then be ventilated.

A halved copper grid was inserted in the microscope. The grid was moved upwards (Fig. 18 f) until it touched the specimen. The GIS was again used to weld the specimen together with the grid (Fig. 18 g) and the Omniprobe was removed after being cut away (Fig. 18 h). The specimen was thinned from both sides. The current was decreased the thinner the specimen became and at the end it was as low as 100 pA. A tilt of 53° was used at the end in order to prevent the formation of a more wedge shaped specimen. Finally the specimen was thin enough to be used in the TEM (Fig. 18 i).

4.4 APT specimen production

The inserts were cut into 150 μm thick slices with a high speed saw. A low speed saw was used to cut rods with a square cross-section from the slices. The rod was dipped in Lacomite, a highly viscous lacquer that sets within half an hour. The dipping and setting process was repeated two to four times so that a lacquer sphere with a approximate diameter of 3-4 mm covered the tip of the rod (Fig. 19). An electrolyte consisting of 5 % H_2SO_4 in ethanol was cooled to -30 °C. The specimen was put in the electrolyte with a counter electrode made from a gold wire formed as a ring around it (Fig. 20). The electropolishing was performed at 29 V and a waist was soon formed at the level of the counter electrode. Within a few minutes, the Lacomite part of the rod fell off. An oxide layer was formed at the tip of the specimen at the final seconds of the electropolishing due to the high current. This layer was removed with a controlled back-polishing method [46]. An electrolyte consisting of 5 % H_2SO_4 in methanol was cooled to -20 °C. With a platinum foil counter electrode, the specimen was given one to three 10 ms pulses of 20 V. This procedure removed the oxide layer but unfortunately made the tip a little more blunt. To get it sharp, it was given 8×2 ms, 8×1 ms and 8×0.5 ms pulses of 20 V.

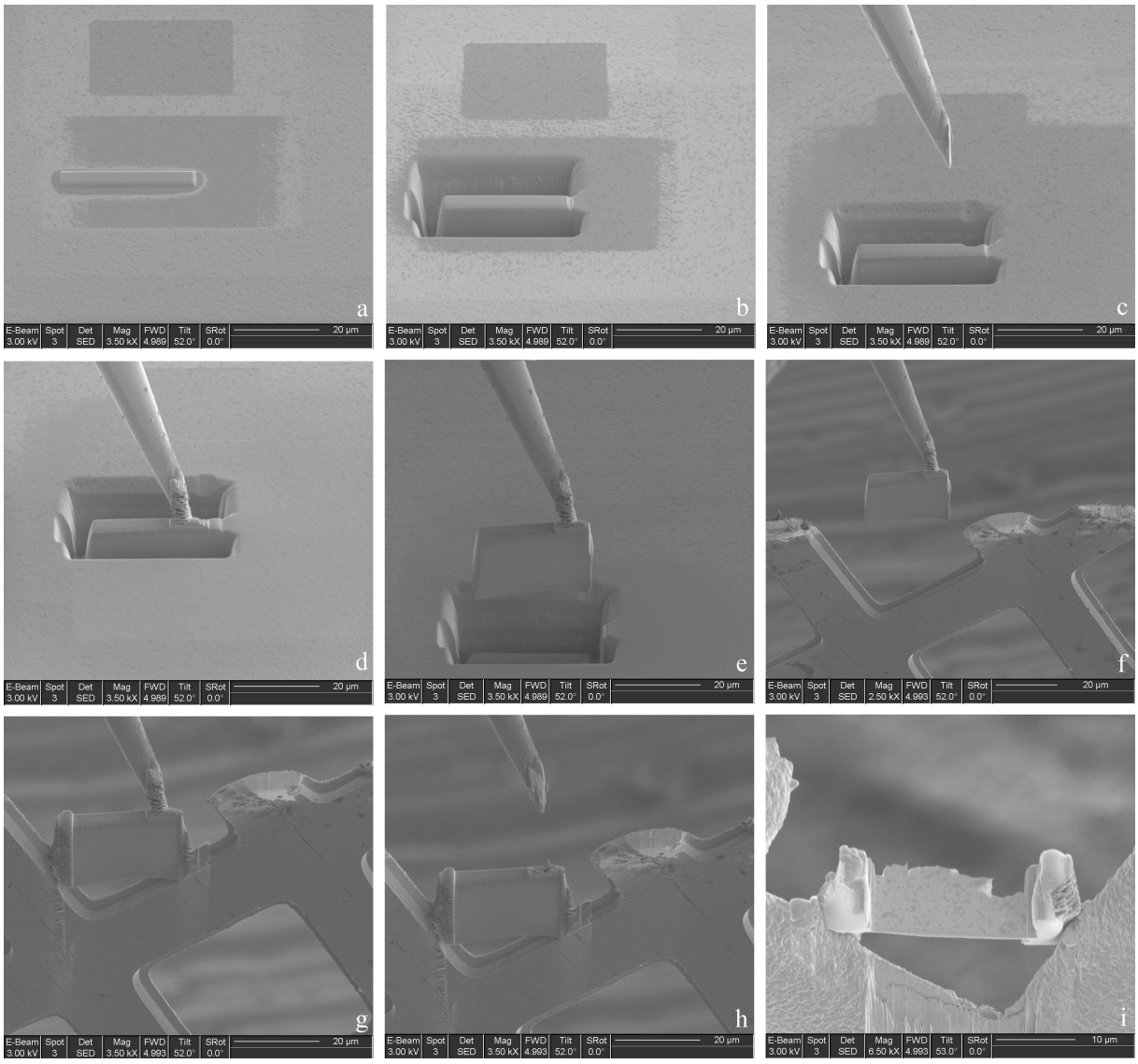

Figure 18: SEM images of a lift-out.

For the first series of materials, it was possible to use the mentioned back-polishing method to bring a WC/WC grain boundary to the tip of the specimen. Pulses approximately 155 μs long were applied to the specimen, each removing 10-20 nm material in the specimen axis direction. The specimen was then checked in a Jeol 2000FX TEM and the distance from the tip to the nearest grain boundary was measured. This procedure was repeated until a grain boundary was present within the outer 50 nm of the tip (Fig. 21). With these short pulses, the specimen sometimes also got more blunt.

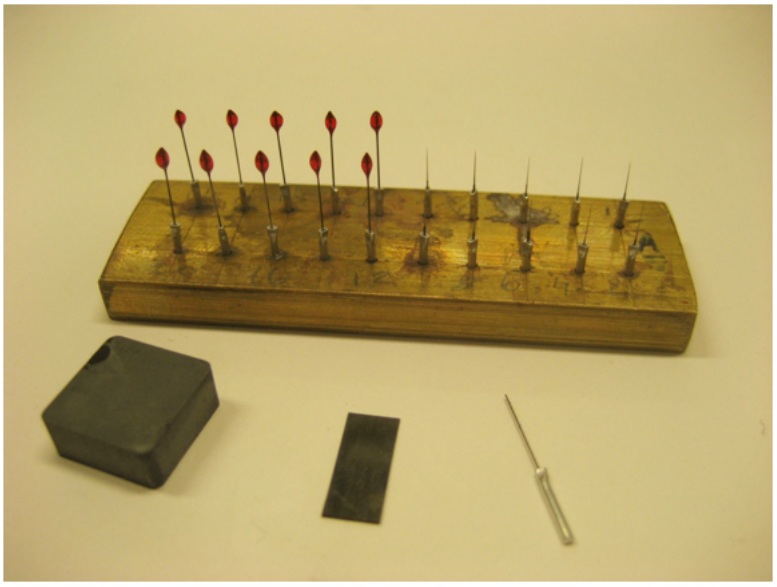

Figure 19: Parts in the production process of APT specimens.

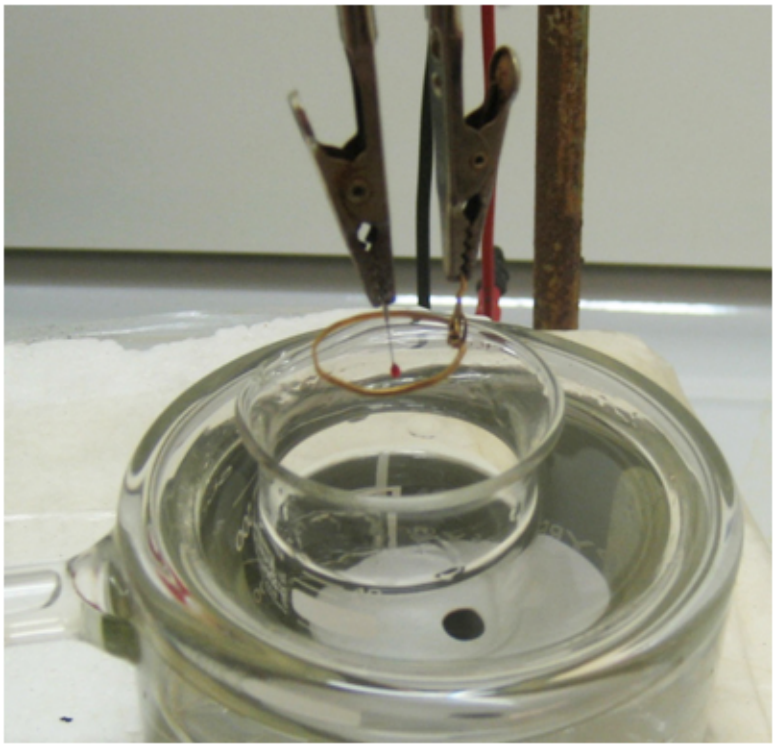

Figure 20: Electropolishing of an APT specimen.

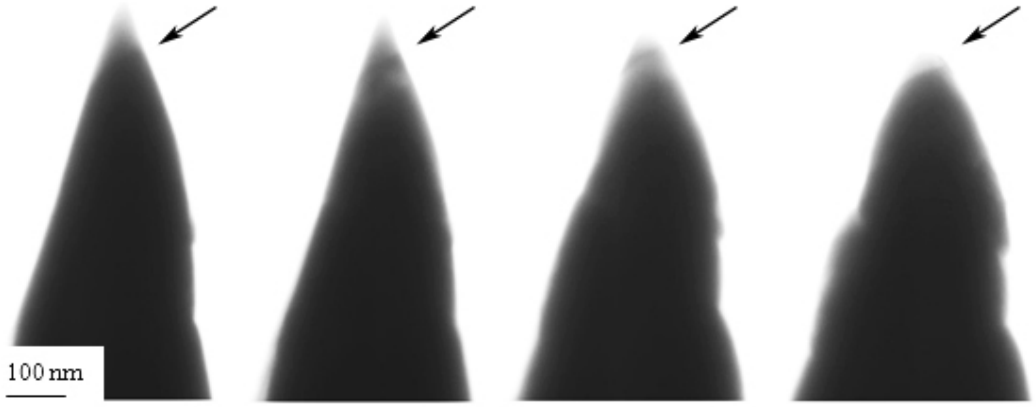

Figure 21: TEM images of a back-polished APT specimen with WC/WC grain boundary after 0, 3, 6 and 7 pulses. The arrows show the location of the grain boundary.

During the electropolishing, as well as during the back-polishing, the binder phase was removed at a much faster rate than the WC phase and thereby making it almost impossible to get a WC/binder phase boundary at the tip of the specimen. Instead the DualBeam workstation was used. The specimen was tilted towards the 30 kV Ga^+ ion source and these ions were used to sputter away small volumes of material from the top of the specimen. The specimen was imaged using electrons and the sputtering was stopped when a phase boundary was present within the outer 100 nm of the specimen (Fig. 22). In order to prevent conical multiple tips at the outer region, the sputtered area was chosen to be a circle with a radius at least 3 μm wide. Even if multiple tips thereby were created, these tips were at least 20 μm down the shank, a distance were the field is very low and field evaporation therefore is not believed to happen. Even if the voltage was decreased to 10 kV at the end of the sputtering, radiation damage and gallium implantation will still be seen in the beginning of an analysis. For this reason, the distance to the phase boundary should be large. On the other hand, this increases the risk of specimen failure. Since the field needed for field evaporation of WC is relatively high (58-64 V/nm [47]) in comparison with Co (37 V/nm [48]), the specimen had to be produced in such way that the analysis will start in the binder phase and then continue in the WC phase. From a field evaporated specimen it can be seen that the binder phase field evaporates easier than WC (Fig. 23) and thus attains a larger tip radius.

For the second series of materials, the additional phase made it difficult to get specimens sharp enough with only electropolishing and controlled back-polishing. Therefore, the DualBeam was used also for the sharpening. For production of specimens with a WC/WC grain boundary at the tip, the specimen was inserted in a FEI Tecnai G2 TEM for measurement of the distance between the tip of the specimen and the closest WC/WC grain boundary between the sputtering treatments.

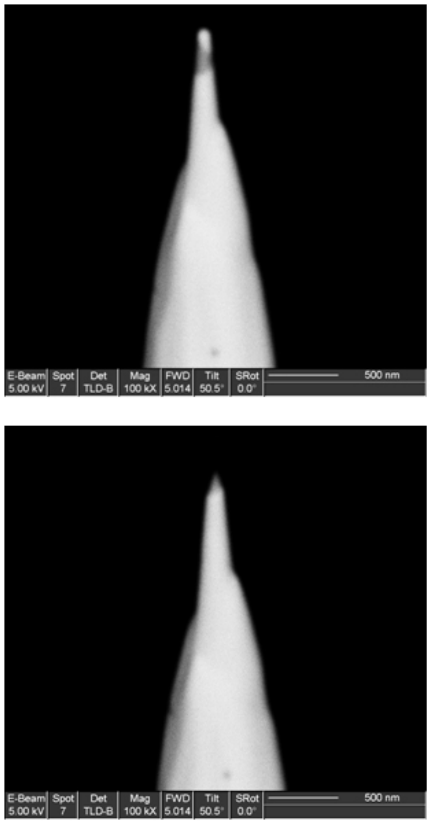

Figure 22: Production of an APT specimen with a binder/WC phase boundary. The upper left image is a SEM micrograph showing the specimen before sputtering. The lower left image show the same specimen after sputtering. The right image is a TEM micrograph after sputtering.

4.5 APT parameters

Two different APT instruments were used, a Cameca EcoTAP and an Imago LEAP 3000X HR.

The Cameca instrument only provided voltage pulsing. The cryostat temperature was chosen to 90 K as a tradeoff between the risk of preferential field evaporation and increased risk of specimen failure. The pulse fraction was with a similar argument set to 20 %. The pulse frequency was 1700 Hz, the maximum for the instrument, and the field evaporation rate 0.5-1.0 % ions per pulse. For FIM, He was used as image gas.

The Imago instrument provided the possibility of both voltage and laser pulsing. It was seen that the risk of specimen fracture was smaller with laser pulsing and therefore this mode was used. The specimen temperature was set to 66 K. First, a laser energy of 0.5 nJ was used but this was found to be too high as molecular ions such as CoH were created.

Figure 23: TEM micrograph of an analysed APT specimen with a WC/binder phase boundary. Note the larger tip radius on the binder phase side.

Therefore, the laser energy was decreased to 0.35 nJ, an energy that might give some Co^+ ions in the beginning of the analysis but no molecular ions. The energy was such that the $12C^+/12C^{2+}$ ratio in WC was 0.35-0.42. The pulse frequency was 200 kHz for most of the analyses. However, when analysing WC/binder phase boundaries in the materials with Zr or Nb, the frequency was decreased to 100 kHz as the heating of the specimen otherwise gives a long tail on the Co^{2+} peak that will disturb the Zr^{3+} or Nb^{3+} signal. The field evaporation rate was 0.5-1.0 % ions per pulse.

For reconstruction, the volume for W atoms was chosen to 10.0374 $Å^3$. Since analyses of WC generally are understoichiometric in terms of C atoms, probably due to field evaporation of several C atoms near each other during the same pulse, the volume of detected C atoms was chosen to 11.144 $Å^3$. For calculation of the number of possible atomic MC planes in WC/binder phase analyses, the atoms were given a 6 nm delocalisation. Two isosurfaces were created, the first where the fraction of W+C atoms were 50 % for calculation of the number of M atoms, and the second where the fraction of W+C atoms were 10 % for measurement of the phase boundary area. The reason for having the second isosurface is that the difference in evaporation field between the binder phase and WC causes an increase in voltage, interpreted by the software as a change in specimen radius.

5 Results and discussion

5.1 Summary of appended papers

Paper I - Effect of V, Cr and Mn additions on the microstructure of WC-Co

Four materials were manufactured, one WC-Co reference material and three materials with 0.5 atomic % additions of Cr, V or Mn. The materials were hardness tested and it was seen that the material with V additions was hardest followed by the material with Cr additions. The WC mean grain size and the fraction of Σ2 WC/WC grain boundaries were measured with EBSD. The material with V additions had the smallest WC grain size and the largest fraction of Σ2 grain boundaries. The materials with Cr or Mn additions had just a little smaller WC grain size than the reference material. However, the material with Cr additions had a higher fraction of Σ2 grain boundaries than the reference material. The results indicate that the Σ2 grain boundaries originate from the powder and are not formed during sintering.

Paper II - Grain and phase boundary segregation in WC-Co with small V, Cr or Mn additions

WC/WC grain boundaries as well as WC/binder phase boundaries in the materials from the previous paper were analysed with EDX in TEM and with APT. It was seen that segregation corresponding to approximately a half monolayer of close packed Co occurs to WC/WC grain boundaries. If Cr, V or Mn is added to the material, these elements segregate to the grain boundaries as well, replacing some of the Co. The results are in agreement with ab initio calculations predicting segregation of these elements [31]-[32]. These calculations also suggests that the segregation improves the strength of the boundaries. For WC/binder phase boundaries, V segregation corresponding to approximately 1.1 atomic layer VC was observed at some interfaces. In the materials with Cr or Mn additions, smaller amounts of Cr or Mn at the phase boundaries were also seen. These results supports the suggestion that the grain growth inhibiting effect is due to a continuous adsorption and desorption of the grain growth inhibiting atoms at the WC/binder phase boundaries during liquid phase sintering [27].

Paper III - Characterisation of WC-Co with cubic carbide additions

Six materials were manufactured, one WC-Co reference material, four materials with TiC, ZrC, NbC or TaC additions and one material with both TiC and ZrC additions. The additions were made so that the as-sintered material would contain 20 volume % cubic carbide. The materials were hardness tested and it was seen that the material with both TiC and ZrC additions was hardest followed by the material with TiC additions and the material

with ZrC additions. The WC and the (M,W)C grain sizes as well as the fraction of Σ2 WC/WC grain boundaries were measured with EBSD. It was seen that all additions inhibited WC grain growth and caused a material with a larger fraction of Σ2 grain boundaries than the reference material. The smallest WC grain size was seen for the materials with TiC additions, followed by the material with TaC, ZrC and NbC additions. A big difference in (M,W)C grain size was seen with the (Zr,W)C grain size being smallest and the (Nb,W)C grain size being largest. The largest fraction of Σ2 grain boundaries were seen in the material with TiC additions followed by the material with both TiC and ZrC additions, the material with NbC additions, the material with ZrC additions and the material with TaC additions. The results, again, indicate that the Σ2 grain boundaries originate from the powder.

Paper IV - Grain and phase boundary segregation in WC-Co with TiC, ZrC, NbC or TaC cubic carbide additions

WC/WC grain boundaries, (M,W)C/WC phase boundaries as well as WC/binder phase boundaries in the materials from the previous paper were investigated with EDX in TEM and with APT. It was seen that segregation corresponding to between a half and one monolayer of close packed Co occurs to WC/WC grain boundaries as well as to (M,W)C phase boundaries. Ti, Zr, Nb, but not Ta, segregate to the grain boundaries and replace Co at the interface. Segregation of Ti to grain boundaries was predicted [32] but the segregation of Zr and Nb was previously not known. What effect the Ti, Zr and Nb segregation has on the material properties are not known. WC/binder phase boundaries showed that Ti, Zr, Nb and Ta segregate to some interfaces. The amount of segregation corresponds to less than one monolayer, assuming a close packed MC film. The observed segregation does not contradict the suggested grain growth inhibiting mechanism [27]. In addition, interfacial segregation of B, P and Fe, present in the material as impurities, was observed.

Paper V - Transition metal solubilities in WC in cemented carbide materials

The solubility in WC of Ti, V, Cr, Mn, Co, Zr, Nb and Ta in the different materials produced for the earlier papers was measured with APT. Ta had the highest observed solubility followed by Nb, Cr and V, all of these with an atomic fraction solubility in the 10^{-3} range. Smaller solubilities were also detected for Ti and Mn. The solubility of Zr and Co was too small to be detected by APT. The experimental results were compared with theoretically calculated solubilities using atomistic modelling with a good agreement in the trend for solubility between the elements. The results from the study should be incorporated in thermodynamic databases for cemented carbides in the future.

Paper VI - Binder phase grain size and binder grain boundary segregation in WC-Co based cemented carbides

The parameters that control the binder phase nucleation after liquid state sintering were investigated by measurement of the binder phase grain size with EBSD. The results indicated that binder phase nucleation is facilitated by a small WC grain size, a small binder phase fraction, a low amount of W dissolved in the binder phase and a low cooling rate. The presence of a cubic carbide phase does not have a large effect on the nucleation. In addition, an EBSD analysis of the material with Cr additions was used to identify a binder phase grain boundary. A TEM specimen including this grain boundary was produced and analysed with EDX in TEM. It was seen that to the investigated boundary, W had segregated.

5.2 General remarks

During this work, it was observed that Co segregated to all analysed WC/WC grain boundaries and WC/(M,W)C phase boundaries. The amount of segregation corresponded in almost all cases to a thickness less than one monolayer of close packed Co. It is thereby concluded that the Co infiltration to the interfaces does not break up the continuous hard phase skeleton. As discussed, this segregation is believed to have a strengthening effect of the material. Depending on the additions to the powder mixture, some of the segregated Co is replaced by Ti, V, Cr, Mn, Fe, Zr, or Nb and this might improve the material properties even further.

It was observed that Ti, V, Cr, Mn, Zr, Nb and Ta segregate to WC/binder phase boundaries and the largest tendency of segregation was seen for V where the segregation corresponded to approximately one monolayer of close packed atoms if a cubic VC is assumed at the interface. The segregation of M atoms to the WC/binder phase boundaries are believed to play an important role in the WC grain growth inhibition process. Our results support a theory where the grain growth inhibition is due to a continuous adsorption and desorption of M atoms at the WC/binder phase boundary.

Earlier, the solubility in WC of transition metals has generally been neglected on the assumption of being small. During this work, it was seen that Ta, Nb, Cr and V has an atomic fraction solubility in the 10^{-3} range. This knowledge should be incorporated in future thermodynamic databases.

5.3 Outlook

The results from this work suggest that the following topics should be studied further:

- Ab initio calculations of what effect Fe, Zr and Nb segregation to WC/WC grain boundaries has on the work of separation of the interface.
- Ab initio calculations of what effect segregation to WC/WC grain boundaries has on the resistance to grain boundary sliding.
- Ab initio calculations of what effect Co segregation to WC/(M,W)C phase boundaries has on the strength of such interfaces.
- Controlled testing at high temperature and load of materials with different additions in order to see if the observed segregation to grain and phase boundaries are beneficial in practice.
- Production of materials with transition metal additions that are different in carbon potential in order to improve the databases for solubilities.

Acknowledgements

I would like to thank everyone that has helped me with and paid interest to the work I've carried out during the last five years. I'm very fortunate for having such supporting family, friends and colleagues. Especially, I would like to thank:

- My supervisor Hans-Olof Andrén for keeping his enthusiasm and support for my research and also my studies in pedagogy. The door has always been open for anything that has crossed my mind. I've got an excellent introduction to the academic world including the art of writing articles and enjoying conferences all around the world.
- My co-supervisors Susanne Norgren from Sandvik and Bo Jansson from Seco Tools for valuable discussions and help with thermodynamic calculations.
- Other participants in the project: Göran Wahnström, Sven Johansson and Mattias Slabanja from Chalmers, Ernesto Coronel, Mattias Elfwing and Per Gustafson from Sandvik, Jenni Zackrisson from Seco Tools and Sabine Lay, Valérie Bounhoure and Jean-Michel Missiaen from INP Grenoble. The collaboration has enabled valuable discussions, interesting visits and great dinners.
- The head of our division and my examiner Eva Olsson for introducing me to the group and for supporting my work with TEM.
- Krystyna Stiller from Chalmers and David Seidman and Dieter Isheim from Northwestern University for giving me the opportunity to learn how to use the laser assisted atom probe at Northwestern University.
- Anders Kvist for keeping the instruments working and being a very good friend at, and outside of, work.
- Ola Löfgren for supporting me with all computer related issues.
- My room-mate Pia Tejland for interesting and amusing discussions, especially those concerning life outside work.
- My parents, my brother and Ellen for all love and support.

Financial support was received from Sandvik Tooling AB, Seco Tools AB and the Swedish Reseach Council (Vetenskapsrådet).

References

[1] B. Aronsson, *The origins and growth of cemented carbide*, Second edition, Ord&Form AB, Uppsala, Sweden, 2005

[2] G. S. Upadhyaya, *Cemented tungsten carbides*, Noyes Publications, Westwood, USA, 1998

[3] H. E. Exner, *Physical and chemical nature of cemented carbides*, International Metals Review, 1979, 4, 149-173

[4] Sandvik Coromant, *Modern skärande bearbetning*, Tofters Tryckeri AB, 1994 (in Swedish)

[5] R. M. German, *Sintering theory and practice*, John Wiley & Sons, USA, 1996

[6] W. D. Schubert, A. Bock, B. Lux, *General aspects and limits of conventional ultrafine WC powder manufacture and hard metal production*, International Journal of Refractory Metals & Hard Materials, 1995, 13, 281-296

[7] H. Fischmeister, G. Grimvall, *Ostwald ripening – a survey* In: G.C. Kuczynski (editor), Materials Science Research, vol. 6, Sintering and related phenomena, Plenum Press, New York, USA, 1973, 119-149

[8] J. Kishino, H. Nomura, S. G. Shin, H. Matsubara, T. Tanase, *Computational study on grain growth in cemented carbides*, Proceedings of the 15th International Plansee Seminar 2001, Editors: G. Kneringer, P. Rödhammer, H. Wildner, Wattens, Austria, 2001, 2, 50-64

[9] B. Roebuck, E. G. Bennett, W. P Byrne, M. G. Gee, *Characterisation of baseline hardmetals using property maps*, NPL Report CMMT(A)172, 1999

[10] W. D. Schubert, H. Neumeister, G. Kinger, B. Lux, *Hardness to toughness relationship of fine-grained WC-Co hardmetals*, International Journal of Refractory Metals & Hard Materials, 1998, 16, 133-142

[11] K. Hayashi, Y. Fuke, H. Suzuki, *Effects of addition carbides on the grain size of WC-Co alloy*, Journal of the Japan Society of Powder Metallurgy, 1972, 19 (2), 67-71

[12] H. Suzuki, Y. Fuke, K. Hayashi, *Grain size of WC in sintered WC-VC-Co alloys*, Journal of the Japan Society of Powder Metallurgy, 1972, 19 (3), 106-112

[13] <http://www.thermocalc.com>; 2008 CCC1 [accessed 100422].

[14] A. Markström, K. Frisk, B. Sundman, *A revised thermodynamic description of the Co-W-C system*, Journal of Phase Equilibria and Diffusion, 2005, 26, 152-160

[15] B. Uhrenius, *Pulvermetallurgi*, Kungliga Tekniska Högskolan, Stockholm, Sweden, 2000 (in Swedish)

[16] J. Vicens, E. Laurent-Pinson, J. L. Chermant, G. Nouet, *Structural analysis and properties of grain boundaries in hexagonal carbides*, Journal de Physique, 1988, 49, 271-276

[17] G. Östberg, M. U. Farooq, M. Christensen, H.-O. Andrén, U. Klement, G. Wahnström, *Effect of $\Sigma 2$ grain boundaries on plastic deformation of WC-Co cemented carbides*, Materials Science and Engineering: A, 2006, 416, 119-125

[18] W. F. Gale, T. C. Totemeier, *Smithells metals reference book*, Eighth eidition, Elsevier Butterworth-Heinemann, Chennai, India, 2004

[19] L. Manlang, H. Xiaoying, D. Shitian, S. Daqin, C. Yumei, Y. Zhenmei, *Diffraction-contrast study of microstructure and deformation process of WC-Co cemented carbide*, International Journal of Refractory Metals & Hard Materials, 1983, 2, 129-132

[20] V. K. Sarin, T. Johannesson, *On the deformation of WC-Co based cemented carbides*, Metal Science, 1975, 9, 472-476

[21] A. Egami, M. Ehira, M. Machida,*Morphology of vanadium carbide in submicron hardmetals*, Proceedings of the 13th International Plansee Seminar 1993, Editors: H. Bildstein, R. Eck, Wattens, Austria, 1993, 3, 639-648

[22] T. Taniuchi, K. Okada, T. Tanase, *Sintering behavior of VC-doped micro-grained cemented carbide*, Proceedings of the 14th International Plansee Seminar 1997, Editors: G. Kneringer, P. Rödhammer, P. Wilhartitz, 1997, 2, 644-657

[23] A. Jaroenworaluck, T. Yamamoto, Y. Ikuhara, T. Sakuma, T. Taniuchi, K. Okada, T. Tanase, *Segregation of vanadium at the WC/Co interface in VC-doped WC-Co*, Journal of Materials Research, 1998, 13, 2450-2452

[24] T. Yamamoto, Y. Ikuhara, T. Sakuma, *High resolution transmission electron microscopy study in VC-doped WC–Co compound*, Science and Technology of Advanced Materials, 2000, 1, 97-104

[25] S. Lay, S. Hamar-Thibault, A. Lackner, *Location of VC in VC, Cr_3C_2 codoped WC-Co cermets by HREM and EELS*, International Journal of Refractory Metals & Hard Materials, 2002, 20, 61-69

[26] S. Lay, J. Thibault, S. Hamar-Thibault, *Structure and role of the interfacial layers in VC-rich WC-Co cermets*, Philosophical Magazine, 2003, 83, 1175-1190

[27] M. Kawakami, O. Terada, K. Hayashi, *Effect of sintering cooling rate on V segregation amount at WC/Co interface in VC-doped WC-Co fine-grained hardmetal*, Journal of the Japan Society of Powder and Powder Metallurgy, 2004, 8, 576-585

[28] T. Yamamoto, Y. Ikuhara, T. Watanabe, T. Sakuma, Y. Taniuchi, K. Okada, T. Tanase, *High resolution microscopy study in Cr_3C_2-doped WC-Co*, Journal of Materials Science, 2001, 36, 3885-3890

[29] A. Delanoë, M. Bacia, E. Pauty, S. Lay, C. H. Allibert, *Cr-rich layer at the WC/Co interface in Cr-doped WC-Co cermets: segregation or metastable carbide?*, Journal of Crystal Growth, 2004, 270, 219-227

[30] G. Östberg, K. Buss, M. Christensen, S. Norgren, H.-O. Andrén, D. Mari, G. Wahnström, I. Reineck, *Mechanisms of plastic deformation of WC–Co and Ti(C, N)–WC–Co* , International Journal of Refractory Metals and Hard Materials, 2006, 24, 135-144

[31] M. Christensen, G. Wahnström, *Effects of cobalt intergranular segregation on interface energetics in WC-Co*, Acta Materialia, 2004, 52, 2199-2207

[32] M. Christensen, G. Wahnström, *Strength and reinforcement of interfaces in cemented carbides*, International Journal of Refractory Metals & Hard Materials, 2006, 24, 80-88

[33] A. Henjered, M. Hellsing, H.-O. Andrén, H. Nordén, *Quantitative microanalysis of carbide/carbide interfaces in WC-Co-base cemented carbides*, Materials Science and Technology 1986, 2, 847-855

[34] D. Williams, B. Carter, *Transmission electron microscopy*, First edition, Plenum Press, New York, 1996

[35] J. Goldstein, D. Newbury, D. Joy, C. Lyman, P. Echlin, E. Lifshin, L. Sawyer, J. Michael, *Scanning Electron Microscopy and X-Ray Microanalysis*, Third edition, Kluwer Academic/ Plenum Publishers, New York, 2003

[36] F. J. Humphreys, *Review grain and subgrain characterisation by electron backscatter diffraction*, Journal of Materials Science, 2001, 36, 3833-3854

[37] FEI Company, *xP DualBeam workstation reference guide*, 1999

[38] G. Ben Assayag, P. Sudraud, *LMIS energy broadening interpretation supported by HV-TEM observations*, Journal de Physique, 1984, 12 C9, 223-226

[39] J. Börjesson, *The role of interfacial microstructure of perovskite thin films - a high resolution and in situ study*, Ph.D thesis, Chalmers University of Technology, Göteborg, Sweden, 2009

[40] FEI Company, *Titan condenser manual*, 2005

[41] M. K. Miller, *Atom probe tomography*, Kluwer Academic / Plenum Publishers, New York, 2000

[42] D. N. Seidman, K. M. Stiller, *An atom-probe tomography primer*, MRS Bulletin, 2009, 34, 717-721

[43] D. G. Brandon, *The structure of high-angle grain boundaries*, Acta Metallurgica, 1966, 14, 1479-1484

[44] L. A. Giannuzzi, F. A. Stevie, *A review of focused ion beam milling techniques for TEM specimen preparation*, Micron, 1999, 30, 197-204

[45] FEI Company, *xP DualBeam system user's guide* Revolution Publishing, 2003

[46] U. Rolander, *A method for sharpening FIM-specimens*, Journal de Physique, 1986, 11 C7, 449-452

[47] H.-O. Andrén, A. Henjered, D. Kingham, *On the charge state of tungsten ions in the pulsed-field atom probe*, Surface Science, 1984, 138, 227-236

[48] T. T. Tsong, *Field ion image formation*, Surface Science, 1978, 70, 211-233